

# Exact solutions to chaotic and stochastic systems

J. A. González<sup>1</sup>, L. I. Reyes<sup>1,2</sup>, and L. E. Guerrero<sup>2</sup>

<sup>1</sup>*Centro de Física, Instituto Venezolano de Investigaciones Científicas, Apartado Postal 21827, Caracas 1020-A, Venezuela*

<sup>2</sup>*Departamento de Física, Universidad Simón Bolívar, Apartado 89000, Caracas 1080-A, Venezuela*

(May 20, 2019)

We investigate functions that are exact solutions to chaotic dynamical systems. A generalization of these functions can produce truly random numbers. For the first time, we present solutions to random maps. This allows us to check, analytically, some recent results about the complexity of random dynamical systems. We confirm the result that a negative Lyapunov exponent does not imply predictability in random systems. We test the effectiveness of forecasting methods in distinguishing between chaotic and random time-series. Using the explicit random functions, we can give explicit analytical formulas for the output signal in some systems with stochastic resonance. We study the influence of chaos on the stochastic resonance. We show, theoretically, the existence of a new type of solitonic stochastic resonance, where the shape of the kink is crucial. Using our models we can predict specific patterns in the output signal of stochastic resonance systems.

Recently, many outstanding papers [1–4] have stated the importance of having true random models. The best existing pseudo-random number generators can yield incorrect results due to the “unavoidable” correlations that appear between the generated values [1–3]. On the other hand, there is a great interest in random dynamical systems [5–7]. In recent years, there has been much discussion about the transition to chaos and the way to characterize predictability and complexity in these systems [6,7]. There is also strong controversy about the existing methods to distinguish chaotic and completely random systems [8–10].

In the present paper we investigate explicit functions that are exact solutions to nonlinear chaotic maps. A generalization of these functions can produce truly random sequences. Even if the initial conditions are known exactly, the next values are in principle unpredictable from the previous values. These functions cannot be expressed as a map of type  $X_{n+1} = g(X_n, X_{n-1}, \dots, X_{n-r+1})$ . Using some of these functions we can exactly solve random maps as the following:

$$X_{n+1} = f(X_n, I_n), \tag{1}$$

where  $I_n$  is a random variable.

We can confirm the result [6,7] that a negative Lyapunov exponent does not imply predictability in random systems. We show that the forecasting methods [8–10] are very effective distinguishing chaos from random time-series. We investigate the influence of the level of chaos on the stochastic resonance (SR). We can give explicit analytical formulas for the output signal of some systems with stochastic resonance. We show the existence of a new type of solitonic stochastic resonance (SSR), where the shape of the kink is crucial.

## I. INTRODUCTION

There is the common believe that, as truly random numbers should be unpredictable in advance, they must be produced by random physical processes such as radioactive decay,

thermal noise in electronic devices, cosmic ray arrival time, etc. [4].

Knowing the past and present values should give no information as to future outcomes of a truly random variable [2]. Thus, a recursive mathematical algorithm should not be able to describe a truly random process. From this, it seems, that deterministic randomness is inherently unattainable [2].

Here we have two problems as a motivation for our work:

1. How to describe theoretically these physical phenomena that are truly random?
2. How to produce truly random numbers, which are necessary in different physical calculations such as Monte Carlo method?

The purpose of our study is to find explicit functions that produce truly random dynamics. These functions can be used as random number generators and as analytical solutions to nonlinear random systems.

It is well-known [11,12] that the function  $X_n = \sin^2(\theta\pi 2^n)$  is the general solution to the logistic map  $X_{n+1} = 4X_n(1 - X_n)$ . Recently, other chaotic maps have been reported to have exact solutions [13–19]. In the present letter we will investigate in detail a generalization of the solution to the logistic map:

$$X_n = \sin^2(\theta\pi z^n), \tag{2}$$

where  $z$  is a real number.

For  $z$  integer, the function (2) is the general solution to the family of maps:

$$X_{n+1} = \sin^2\left(z \arcsin \sqrt{X_n}\right) \tag{3}$$

Even for a real  $z$  we can calculate the Lyapunov exponent of the map (3) exactly:  
 $\lambda = \ln z$ .

For  $z > 1$  the map (3) is chaotic. Nevertheless, for fractionary  $z$  the dynamics contained in function (2) is quite different from that of map (3). In fact, for a fractionary  $z$ , the first-return map generated by (2) is multivalued (see Figures 1 and 2). Let us  $z$  be a rational

number expressed as  $z = p/q$ , where  $p$  and  $q$  are relative prime numbers. Then the first-return map produced by function (2) is a curve such that, in general, for a value of  $X_n$  we will have  $q$  values of  $X_{n+1}$ . On the other hand, for a value of  $X_{n+1}$  we will have  $p$  values of  $X_n$ . Geometrically, these curves are Lissajous figures [17]. But we should note that their meaning here is very different from that in their original definition. In this context, they represent chaotic first-return maps. For  $z$  irrational, the first-return map is a random set of points as shown in Fig. 3.

The paper is organized as follows. In Section II we study the properties of the functions  $X_n = \sin^2(\theta\pi z^n)$ . We present a rigorous proof that, for  $z$  fractionary, the produced sequences are absolutely unpredictable in advance. Moreover, the outcomes are completely independent. In section III we discuss the use of these functions in actual numerical calculations. Section IV is dedicated to random maps of type  $X_{n+1} = f(X_n, I_n)$ , where  $I_n$  is a random variable. The functions (2) can help to find analytical solutions to these maps. We calculate exactly the complexity of a random map. This allows us to check some recent results about the complexity and predictability of random maps. In section V we address the problem of distinguishing chaos from random time-series. For this, we check the effectivity of the so-called “nonlinear forecasting methods”. Section VI is devoted to stochastic resonance (SR). First we give some introductory remarks about the historical arrivements in SR. Considering the fact that we can calculate exactly the Lyapunov exponent of a class of chaotic maps, we are able to investigate the influence of the level of chaos on SR. This is done first in the most common setup for SR: a bistable system. Then, we investigate the so-called nonlinear static systems with SR. For these systems, we can present explicit analytical functions that describe the output of the system. Using the functions we can investigate the actual dynamics of the system. Finally, based on theoretical investigations, we show the existence of a new type of solitonic stochastic resonance, where the shape of the kink is crucial.

## II. EXPLICIT STOCHASTIC FUNCTIONS

After a rigorous analysis of function (2) we arrive at interesting conclusions. For most fractionary  $z > 1$  the function (2) is not only chaotic, but its next value is impossible to predict (from the previous values) unless  $\theta$  is exactly known. When  $z$  is integer, the initial condition  $X_0$  defines univocally the value of  $\theta$  (any value of  $\theta$  out of the interval  $0 < \theta < 1$  defining  $X_0$  is equivalent to one in that interval). If  $z$  is fractionary, this is not so. There exists an infinite number of values of  $\theta$  that satisfy the initial conditions. The time-series produced for different values of  $\theta$  satisfying the initial conditions is different in most cases. The fact that we know the initial conditions does not imply that we can determine  $\theta$ . So the next value is unpredictable.

Let us consider the case  $z = 3/2$  (see Fig. 2). If we wish to calculate  $X_{n+1}$  from the value  $X_n$  we will have two choices:

$$X_{n+1} = \frac{1}{2} \left[ 1 \pm (1 - 4X_n)(1 - X_n)^{1/2} \right] \quad (4)$$

The value  $X_{n+1}$  could be expressed as a well-defined function of the previous values if  $(1 - X_n)^{1/2}$  could be a rational function of the previous values. However, each time we try to do this we meet the same difficulty because the previous values are also irrational functions of the past values. This process can continue up to infinity.

A different way to see this phenomenon is the following. Consider the family of functions

$$X_n^k = \sin^2 [(\theta_0 + k) \pi z^n], \quad (5)$$

where  $\theta = \theta_0 + k$ ,  $k$  is integer.

For all  $k$ , the time-series  $X_n^k$  ( $k$  fixed,  $n$  as time) have the same initial conditions. If  $z$  is integer, the initial condition defines the complete sequence (see Table I). However, for  $z$  fractionary all the time-series are different. This is because the period of function  $X_n^k$  (now  $n$  is fixed and  $k$  is variable) is different for different  $n$  (for instance, when  $z = 3/2$ , the period of  $X_n^k$  is  $2^n$ ). In general, for  $z = p/q$ , the period is  $q^n$ . That is,  $X_{n+1}$  cannot

be determined by  $X_n$ . Moreover,  $X_{n+1}$  cannot be determined by any number of previous values. Let us see the following example with  $z = 3/2$ . Suppose  $X_n = 0$ . Now we have two possibilities  $X_{n+1} = 0$  or  $X_{n+1} = 1$  (see Table II). Assume  $\theta_0 = 0$  and  $n = 0$ . For any  $\theta = k$  ( $k$  integer),  $X_n = 0$ . Now,  $X_{n+1} = \sin^2 [(3/2)k\pi]$ . So,  $X_{n+1} = 0$  for  $k$  even, and  $X_{n+1} = 1$  for  $k$  odd. But there is no way we can know  $k$  from the statement  $X_n = 0$  (for all  $k$  integer this statement is true). This uncertainty about the next value is present for all points  $X_n$  except  $X_n = 1/4$  and  $X_n = 1$ . But these two points are a set of zero measure. That is, for almost all the points in the interval  $0 < X_n < 1$ , the next value is unpredictable.

For  $z$  irrational there are infinite possibilities for  $X_{n+1}$ . All values are unpredictable. But let us continue with the simple case  $z = 3/2$ . Suppose now that  $\theta = 2^m$ , where  $m$  is integer. Note that in this case  $X_0 = 0$ . But, unless we know  $\theta$ , we never will know when the value  $X_{m+1}$  will be equal to 1 (see Table II). We can have a string of  $m + 1$  zeros ( $m$  can be as large as we wish) and only in the point  $X_{m+1}$  the sequence changes from a string of zeros to the value 1. So, for any finite number  $m + 1$  of previous values  $X_0, X_1, X_2, \dots, X_m$ ; the next value is not defined by the previous values. Note that in this example we can have a string of zeros, but this is because the value  $X_n = 0$  is a pseudo fixed point of the map  $(X_n, X_{n+1})$  due to the intersection of the graph in Fig. 2a with the line  $X_{n+1} = X_n$ . However, in general, the sequence is very stochastic. On the other hand, the uncertainty about which is the next value remains for all the points in the interval  $0 \leq X_n \leq 1$  except for  $X_n = 1/4$  and  $X_n = 1$ . The general uncertainty increases for  $p > q > 2$  (see Table III). In this case, the unpredictability is true for all values of  $X_n$ .

On the other hand, if  $z$  is irrational, then the points on the first-return map  $(X_n, X_{n+1})$  will fill the square  $0 \leq X_n \leq 1; 0 \leq X_{n+1} \leq 1$  (see Fig. 3 and Table IV). For a large but finite number  $n$ , the map is an erratic set of points (we should exclude the numbers of type  $z = m^{1/k}$ , where  $m$  and  $k$  are integers, because in this case the sequence is predictable given  $k$  previous values).

Note that we can consider  $X_n^k$  defined by (5) as an infinite matrix, where the ‘‘columns’’ are the stochastic sequences (dependence on  $n$ ) and the horizontal ‘‘rows’’ are periodic (or

quasiperiodic for irrational  $z$ ) sequences that represent the dependence on  $k$ . For  $z = p/q$ , the “rows” are periodic sequences with period  $q^n$  (see Tables II and III). We see that all the row-sequences have different periods. So, all the column-sequences are generally different. However, for each integer  $m$ , there is an infinite set of columns having a string of values of length  $m$  that is identical in each number of this set. That is, in the matrix  $X_n^k$ , given an initial string of length  $m = 2$ , we will find a string identical to it with a period  $q^2$ . Note (in Table II) that the string  $(0, 1, 1/2)$  can be found in infinite columns. However, the next value is always uncertain. It can be  $X_3 = 0.1464\dots$  or  $X_3 = 0.8536\dots$ . Just to know that the previous values are  $(0, 1, 1/2)$  does not give us the knowledge to determine the next value. The string  $(0, 1, 0, 5, 0.8536\dots, 0.0381\dots, 0.9157\dots, 0.8865\dots, 0.0711\dots, 0.8448\dots, 0.9687\dots)$  can be found with period  $2^9$ . That is, the column number  $2^9 + 1$  possesses this same string. However, the value  $X_{10}$  is not always  $X_{10} = 0.7544\dots$ . It can be  $X_{10} = 0.2455\dots$  with the same probability.

In general, given an initial string of length  $m$ , we will find a string identical to it with a period  $q^m$ . At the same time, most of these strings possess different next values (we have seen a striking example in the text above). Suppose there is a univalent function  $X_{n+1} = g(X_n, X_{n-1}, \dots, X_{n-r+1})$  that is equivalent to the sequence (2) for  $z$  fractionary. If we have more than one sequence  $X_0, X_1, X_2, \dots, X_{m-1}$  with different next values, then we should decide that the map we are looking for cannot be of order  $m$ . If for any  $m$ ,  $m = 1, 2, 3, \dots, \infty$ ; we have more than one sequence  $X_0, X_1, X_2, \dots, X_{m-1}$ , such that the next values are different, then such a map does not exist.

In the text above we have shown that for each string of values  $X_0, X_1, X_2, \dots, X_{m-1}$ , there is another sequence with these same values but with different proceeding values.

For  $z$  irrational, all the row-sequences are quasiperiodic and different. The column-sequences correspond to completely random sequences. These functions can produce a set of completely independent values.

### III. RANDOM NUMBER GENERATORS

Now we should say some words about the use of these functions in actual numerical calculations. The argument of function (2) increases exponentially. So, there can be some problems in generating very large sequences. A practical solution is to change parameters  $\theta$  after a fixed number  $n = N$  of sequence values  $X_n$ . Suppose  $N$  is a number for which there are not calculation problems. For producing the new set of values of  $X_n$  (with a new  $\theta$ ) we start again with  $n = 0$ . This procedure can be repeated the desired number of times (remember that even if the sequence is finite, it will be unpredictable; and a sequence formed as a set of unpredictable sequences will be also unpredictable. It can be shown that there exists always a  $\theta$  such that, with it, the original function will produce the same sequence as that generated with the procedure of changing  $\theta$ ).

For the calculation of truly random numbers with function (2) the best way is to use an irrational  $z$ . This irrational  $z$  has not to be a large number. For instance, we can use  $z = \pi$ . The geometrical place of the return map for  $z$  irrational is the whole square  $0 \leq X_n \leq 1$ ;  $0 \leq X_{n+1} \leq 1$ . So, we do not have to worry about the method for determining the next value of  $\theta$ . For example, we can use the following method in order to change parameter  $\theta$  after each set of  $N$  sequence values.

Let us define  $\theta_s = A W_s$ , where  $s$  is the order number of  $\theta$  in such a way that  $s = 1$  corresponds to the  $\theta$  used for the first set of  $N$  values  $X_n$ ;  $s = 2$  for the second set, etc.;  $W_s$  is a “stochastic” sequence. For instance, the values  $W_s$  can be obtained from the same sequence  $X_n$ . The inequality  $A > 1$  should hold in order to keep the absolute unpredictability.

Another important question about good random numbers is to have a generator able to produce uniformly distributed points. By means of the transformation  $Y_n = (2/\pi) \arcsin(X_n^{1/2})$ ; we can obtain random numbers uniformly distributed on the interval  $(0, 1)$  [19]. Once we have uniformly distributed random numbers, we can use well-known transformations to generate random numbers with any given distribution [19].

We have performed several standard statistical tests with the functions  $X_n = \sin^2(\theta\pi z^n)$

(after the transformation  $Y_n = (2/\pi) \arcsin(X_n^{1/2})$ ). Among them are the following: the central limit theorem test, the moments calculations, the variance calculation and the  $\chi^2$  test. The sequence  $Y_n$  has passed all these tests satisfactorily. For instance, the theoretical values for the moments and variances are the following:  $\langle X^n \rangle = \frac{1}{n+1}$ ,  $\sigma_n = \frac{n^2}{(2n+1)(n+1)^2}$ , and these values are obtained when we use the sequence  $Y_n$ .

The autocorrelation function  $C_m = \langle Y_i Y_{i+m} \rangle - \langle Y_i \rangle^2$  (where  $\langle \dots \rangle$  is the average over all  $i$  with  $i = 1, 2, 3, \dots$ ) can be shown to be zero even for  $m = 1$ . For the known chaotic maps (which sometimes are used as pseudorandom number generators)  $|C_m|$  decays with  $m$ , but there is a range of this dependence that is related to the correlation or memory time.

Recently [21] a new method has been developed, which allows us to compare the randomness of different sequences. In these works, a measure of randomness (we will call it  $R$ ) is introduced.

Suppose we have a sequence of values  $U_1, U_2, U_3, \dots, U_n$ . Form a sequence of vectors

$$X_{(i)} = [U_i, U_{i+1}, \dots, U_{i+m-1}] \quad (6)$$

Now, we will define some variables:

$$C_i^m(r) = \frac{\text{number of } j \text{ such that } d[X_{(i)}, X_{(j)}] \leq r}{N - m + 1} \quad (7)$$

where  $d[X_{(i)}, X_{(j)}]$  is the distance between two vectors, which is defined as follows:

$$d[X_{(i)}, X_{(j)}] = \max(|U_{i+k-1} - U_{j+k-1}|) \quad (8)$$

with  $k = 1, 2, \dots, m$ .

Now we can define the measure of randomness:

$$R(m, r, N) = \phi_{(r)}^m - \phi_{(r)}^{m+1} \quad (9)$$

where

$$\phi_{(r)}^m = \frac{1}{N - m + 1} \sum_{i=1}^{N-m+1} \ln C_i^m(r) \quad (10)$$

This measure depends on the resolution parameter  $r$  and an “embedding” parameter  $m$ . This technique has been proved to be very effective in determining system randomness [21].

For given  $r$  and  $m$  we have a maximum possible randomness. A sequence with maximum randomness is uncorrelated. The randomness of our sequences  $Y_n$  with  $z$  irrational is the maximum possible for the given  $r$  and  $m$ . For instance, if  $r = 0.025$ , the maximum possible randomness is  $R = \ln 40$ . The randomness of function (2) with  $z = \pi$  approaches the value  $R = 3.688$  for increasing  $N$ . For comparison, the randomness of the logistic map at the point of full chaos is  $R = 0.693$ . Even if we further decrease  $r$  and increase  $m$  and  $N$ , for the logistic map and other usually chaotic maps,  $R$  saturates and remains constant.

On the other hand, for  $r \rightarrow 0$ , the randomness of function (2) with  $z = \pi$  tends to the maximum possible value, i.e.  $R \rightarrow \ln(1/r)$ . For  $r \rightarrow 0$ , it never saturates.

We should say that the pseudorandom number generators described in Ref. [1] can pass some of the statistical tests devised to check pseudorandomness [4]. However, hidden errors in these generators have been found [1]. Several researchers have traced the errors to the dependence in the pseudorandom numbers. Indeed, they are all based on recursive algorithms.

Recently simulations of different physical systems have become the “new tests” for pseudorandom number generators. Among these systems are the following: two dimensional Ising model, the ballistic deposition, and random walks. Nogués *et al* [3] have found that using common pseudorandom number generators, the produced random walks present symmetries, meaning that the generated numbers are not independent. On the other hand, the logarithmic plot of the mean distance versus the number of steps  $N$  is not a straight line after  $N > 10^5$  (in fact, it is a rapidly decaying function).

D’Souza, Bar-Yam and Kardar [2] use ballistic deposition to test the randomness of pseudorandom number generators. They found correlations in the pseudorandom numbers and strong coupling between the model and the generator (even generators that pass extensive statistical tests).

In a ballistic deposition model of growth, free particles initiated at random positions

above a one dimensional substrate, descend ballistically and stick upon first touching the surface of the growing cluster. The substrate of length  $L$ , consists of discrete columns indexed by integer values of  $x$ , with  $1 \leq x \leq L$ . The growth interface is defined by the maximum occupied site along each column  $h(x, L)$ , where  $h(x, L)$  also takes on discrete values.

The width of the growth interface  $\xi_L(t)$  on average increases following a power law behavior until reaching a steady asymptotic value, the magnitude of which depends on the underlying substrate size  $L$ . For  $\xi_L(t)$  we have the formula

$$\xi_L^2(t) = \frac{1}{L} \sum_{x=1}^L [h(x, t) - \langle h(t) \rangle]^2 \quad (11)$$

where  $\langle h(t) \rangle$  is the mean height of the surface at time  $t$ .

One consequence of the Kardar-Parisi-Zhang theory is that the steady state behavior for the interface fluctuations in one dimension should resemble a random walk, i.e.,  $\xi_L(t \rightarrow \infty) \sim L^{1/2}$ . Thus, a random walk again serves as a good test for random numbers. These two papers [2,3] have been cited by Fisher [3] in his article about the great problems of statistical physics for this century.

With our numbers  $Y_n$ , the produced random walks possess the correct properties, including the mean distance behavior  $\langle d^2 \rangle \sim N$  (see Fig. 4).

#### IV. RANDOM MAPS

The functions (2) are important not only for numerical simulations. They are relevant by themselves as theoretical paradigms of stochastic processes [4]. Considering the fact that these are explicit functions, we can use them to solve (analytically) many theoretical problems in stochastic dynamical systems.

Consider the following random map [6]:

$$X_{n+1} = \frac{1}{2} \left[ 1 + I_n (1 - 4X_n) (1 - X_n)^{1/2} \right], \quad (12)$$

where  $I_n$  is a random variable that takes the values  $\pm 1$  with equal probability.

An exact solution to this random map can be written as follows:

$$X_n = \sin^2 [\theta\pi (3/2)^n] \quad (13)$$

Now we can check some of the results discussed by the authors of Ref. [6,7]. They have introduced a measure of complexity  $K$  in terms of the average number of bits per time unit necessary to specify the sequence generated by the system. In dynamical systems of type (1) ( (12) is an example) this measure coincides with the rate  $K$  of divergence of nearby trajectories evolving under two different realizations of the random variable  $I_n$ .

The complexity of the dynamics can be measured as

$$K = \lambda\theta(\lambda) + h, \quad (14)$$

where  $\lambda$  is the Lyapunov exponent of the map,  $h$  is the complexity of  $I_n$ , and  $\theta(\lambda)$  is the Heaviside step function. Complexity  $h$  should be defined also as the average number of bits per time unit necessary to specify the random variable  $I_n$ . When  $I_n$  is a usual chaotic noise, then  $h$  coincides with the Kolmogorov-Sinai entropy.

In the case of the random map (12)  $\lambda = \ln(3/2)$  and  $h = \ln 2$ . Hence,  $K = \ln 3$ . On the other hand, any calculation (theoretical or numerical) of  $K$  for the dynamics generated by function (13) yields the correct value  $K = \ln 3$ . Moreover, even an independent calculation of the complexity of this dynamics using different methods [20,21] produces the same result.

Using the functions (2) we can also solve the map

$$X_{n+1} = \frac{1 + I_n\sqrt{1 - X_n}}{2}, \quad (15)$$

where  $I_n$  is defined as in (12).

Here the Lyapunov exponent is negative:  $\lambda = \ln(1/2) < 0$ . However, the complexity is positive:  $K = \ln 2$ .

In the presence of random perturbations,  $K$  can be very different from the standard Lyapunov exponent and, hence, from the Kolmogorov entropy computed with the same realization of the randomness.

We stress that a negative value of  $\lambda$  does not imply predictability.

In general, if we apply the measure of complexity  $K$  to our functions (2), then we obtain the following results: for  $z = p/q$  ( $p$  and  $q$  relative primes),  $K = \ln p$ . If  $z$  is irrational, the complexity is infinite!

We should say that using functions (2) we can create complete sets of orthogonal elements. In the same way that we can solve, to begin with, any map of type  $X_{n+1} = f(X_n)$ , we can also solve theoretically many important problems in stochastic dynamical systems.

## V. NONLINEAR FORECASTING METHODS

Now we address the problem of deciding which of the proposed methods [8–10] for distinguishing chaos from random time-series are more effective. Recently a new method based on nonlinear forecasting was proposed [8–10]. The idea of the method is as follows. One can make short-term predictions that are based on a library of past patterns in a time-series (the method of nonlinear forecasting is described in [8–10] and the references quoted therein). By comparing the predicted and actual values, one can make distinctions between random sequences and deterministic chaos.

For chaotic (but correlated) time-series, the accuracy of the nonlinear forecast falls off with increasing prediction-time interval. On the other hand, for truly random sequences, the forecasting accuracy is independent of the prediction interval. The decrease with time of the correlation coefficient between predicted and actual values can be used to calculate the largest positive Lyapunov exponent of the time-series [9].

The functions (2) are a very good model-system to check this and other methods. In fact, for  $z$  integer, these are chaotic sequences of type:  $X_{n+1} = f(X_n)$ . For  $z = m^{1/k}$ , we have chaotic maps of type:  $X_{n+1} = g(X_n, X_{n-1}, \dots, X_{n-k+1})$ . For  $z$  fractionary, we have different types of random sequences with different complexities. Finally, for  $z$  irrational (generic), the sequence is maximally random.

Suppose we have a sequence  $U_1, U_2, \dots, U_N$ . Now we construct a map with the dependence

$U_n^{predicted}$  as a “function” of  $U_n^{observed}$ .

If we have a correlated chaotic sequence, this dependence is a straight line, i.e.  $U_n^{predicted} \approx U_n^{observed}$  (when the forecasting method is applied for one time step into the future). When we increase the number of time steps into the future, this relation deteriorates. When we apply this method to function (2) with  $z = \pi$  (after transformation  $Y_n = (2/\pi) \arcsin \sqrt{X_n}$ ), even the map  $U_n^{predicted}$  vs  $U_n^{observed}$  for one time step into the future is a map equivalent to that shown in Fig. 5. On the other hand, the correlation coefficient is independent of the prediction time. In fact, there are no correlations. The details will be given elsewhere. Nevertheless, we should say that this method is quite efficient in distinguishing chaos from randomness. However, it cannot distinguish between different random time-series.

Other methods discussed in [8], are less effective in this task. They are more qualitative, requiring subjective judgement about whether there is an attractor of given dimensions.

## VI. STOCHASTIC RESONANCE

### A. Lyapunov exponents

A phenomenon that has awakened very much interest in last years is stochastic resonance (SR) [22–40]. The classical model for this phenomenon is the following:

$$\dot{x} - x + x^3 = A_0 \sin(\omega t) + \eta(t). \quad (16)$$

The sum of a noise signal,  $\eta(t)$ , and a weak periodic signal is used to drive a bistable system. The most important characteristic of SR is that the signal-to-noise ratio (SNR) has a maximum in the plot SNR vs  $D$ , where  $D$  is the noise intensity, for a finite nonzero value of the noise intensity.

It has been shown that SR still occurs when chaos, rather than noise, is used as the nonperiodic component of the driving signal [27]. Several authors have investigated the SR in chaotic systems [27–32].

A very important question is how SR depends on the largest Lyapunov exponent of the driving chaotic noise [25]. We address this problem systematically for the first time, since we can solve exactly the problem of calculating the Lyapunov exponent. We should say that for large values of the Lyapunov exponent, the SR is not a very sensitive phenomenon on the level of chaos (this is unlike the phenomena discussed in Ref. [1–3]). The curve SNR vs  $D$  practically has no variation for  $\lambda \gg \ln 3$ . However, in the interval  $\ln(3/2) < \lambda < \ln 2$ , the SR strongly depends on the Lyapunov exponent. In this interval, the maximum of SNR is shifted to the right (larger noise intensities) and is amplified!. Figure 6 shows the dependence  $SNR(D)$  for different values of the Lyapunov exponent  $\lambda$ . These data are the result of numerical simulations of equation (16). We can compare this result with that obtained in Ref. [33]. In this work, the phenomenon of stochastic resonance is studied in the presence of colored noise. In overdamped systems, the authors find that SR is suppressed with increasing noise colour. In contrast, for colored noise induced by inertia (as well as for asymmetric dichotomic noise), they obtain an enhancement of SR.

The same result can be obtained in the so called threshold systems [34–36]. For instance, define

$$I_n = g(p_n + \eta_n), \quad (17)$$

where  $p_n$  is a periodic function,  $\eta_n$  is some kind of noise, and  $g(x)$  is a function with some properties that allow the existence of SR [34–36].

The simplest case is the following:

$$g(x) = \begin{cases} -V, & x < x_{th}, \\ V, & x > x_{th}. \end{cases} \quad (18)$$

A nonlinear circuit with this kind of threshold nonlinearity is discussed in [36].

Different measures have been used to characterize stochastic resonance. In particular, in Ref. [41] the dynamics of noisy bistable systems is analyzed by means of Lyapunov exponents and measures of complexity.

It can be shown that, in stochastic resonance systems, the function  $K(D)$  (where  $K$  is the complexity as defined above and  $D$  is the noise intensity) has a local minimum for a

nonzero value of  $D$ . This minimum represents an optimal value of noise intensity at which SR occurs. This result confirms the findings of Ref. [41].

We can consider  $K$  as a “dynamical measure” of SR because  $K$  coincides with the rate of divergence of nearby trajectories evolving under two different noise realizations.

This measure can be used to characterize more general stochastic dynamical systems as the following:

$$X_{n+1} = F(X_n, p_n, \eta_n), \quad (19)$$

where  $p_n$  is a periodic function and  $\eta_n$  is the noise.

Let us investigate a particular example:

$$X_{n+1} = \cos \left\{ \left[ 1 + \varepsilon (p_n + D\eta_n)^2 \right] \arccos (X_n) \right\}. \quad (20)$$

Here  $p_n$  is a periodic function of amplitude  $\alpha$  and  $\eta_n$  is a chaotic noise defined as follows:

$$\eta_n = Y_n - \delta - 1, \quad (21)$$

where  $\delta$  is a parameter for which  $0 < \delta < 1$  and  $Y_{n+1} = \sin^2 \left( z \arcsin \sqrt{Y_n} \right)$ .

For this dynamical system, function  $K(D)$  has a minimum for a finite  $D$ .

Let us suppose that  $p_n$  is a period-one function. We can write down an analytic expression for  $K$ :

$$K = \ln \left\{ z \left[ 1 + \frac{\varepsilon}{2} \left( (\alpha - D\delta)^2 + (\alpha - D(z-1))^2 \right) \right] \right\}. \quad (22)$$

The function  $K(D)$  is shown in Fig. 7. For a fixed  $z$ , the minimum of  $K$  is obtained approximately for  $D = \alpha/(z-1)$ . If we minimize  $K$  with respect of both  $D$  and  $z$ , we obtain  $D = \alpha/\delta$ ,  $z = 1 + \delta$ .

Note that for  $1 + \delta < z < 3$ , the minimum is deeper and is shifted to the right as  $z$  is decreased. This is a phenomenon similar to that obtained using SNR in Fig. 6. See also subsection VI-E, where some experiments are mentioned.

We should say that  $K$  can characterize the dynamics of dynamical systems of type (19) even when there is no periodic function at all.

In some cases, for a finite value of  $D$  we can find the least complex dynamics.

In some sense, this is a more general phenomenon than the usual stochastic resonance. In fact, this is an example of the so-called noise-induced disorder-order transitions, of which the SR phenomena can be a subset.

In Fig. 8, different time-series and return maps produced by the dynamical system (20) are shown. Note that for some intermediate value of  $D$  we obtain the least complex dynamics.

In Fig. (9) we see that when both  $D$  and  $z$  are very close to the optimal values, then the resulting dynamics is very predictable.

Note that this system can be chaotic even when  $D = 0$ , due to the intrinsic nonlinear dynamics of the system. However, for some finite value of the noise intensity  $D > 0$ , we can control this chaotic dynamics. So, in this case, we are truly controlling the chaotic system using chaotic noise.

## B. Explicit output functions for SR systems

Recently scientists have learned that stochastic resonance can appear not only in bistable systems [36–38]. A very interesting class of systems is that of the so called nonlinear static (or “nondynamical”) systems. In Ref. [36–38] a theory of these systems is presented. Using this theory and our functions (2) we can write down an explicit “solution” function to these systems. For instance, the function:

$$I_n = \tanh \{B [A_0 \sin (\omega n) + D \cos (\theta \pi z^n) - V_{th}]\} \quad (23)$$

can behave as a SR system. Figure 10 shows that the function (23) is a SR system for  $B = 24$ . For  $B = 1$  the stochastic resonance disappears. Here the SNR was calculated numerically using function (23) as the output signal. In fact, we can construct a very general class of SR functions of type  $I_n = g(V_n) + \xi_n$ , where  $V_n = p_n + \eta_n$  is the input and  $I_n$  is the output. Function  $\xi_n$  represents the intrinsic noise [38].

Note that although the systems described in Ref. [36–38] are called “static systems”, once we have constructed our explicit functions, e.g. Eq. (23), we can obtain exact solutions to very dynamical systems. Also note that it is very easy to check that there is a maximum in the dependence SNR vs  $D$ ; however our explicit functions can be investigated using mathematical analysis, not only statistics. Very different functions with very different dynamics can have the same SNR behavior and other statistical properties. Using our explicit functions we can investigate the true dynamics of the system.

The analysis of functions (2) allows us to construct a continuous and differentiable function with properties similar to those of the chaotic functions (2). Let us give an example:

$$f(t) = \sin\{B_1 \sinh [a_1 \cos(\omega_1 t) + a_2 \cos(\omega_2 t)] + B_2 \cosh [a_3 \cos(\omega_3 t) + a_4 \cos(\omega_4 t)]\} \quad (24)$$

Using functions of this kind we can find analytic solutions to continuous chaotic dynamical systems. Function (24) with the parameter values  $B_1 = 20, B_2 = 30, a_1 = 10, a_2 = 15, a_3 = 10, a_4 = 15, \omega_1 = 1, \omega_2 = \pi, \omega_3 = \sqrt{2}, \omega_4 = e$ ; behaves as a chaotic system (see Fig. 11). Any investigation (theoretical or numerical) will give the same result: the maximum Lyapunov exponent is positive. Moreover, if we need a continuous dynamics with a chaotic gaussianlike “noise” we can use a transformation of (24):  $g(t) = \ln [f^2(t)/(1 - f^2(t))]$ . We have been able to produce SR with function (24),  $f(t)$ , and  $g(t)$ . In Fig. 12 SNR is calculated from numerical simulations of equation (16) and using the continuous chaotic function  $g(t) = \ln [f^2(t)/(1 - f^2(t))]$ , where  $f(t)$  is defined by equation (24).

### C. Solitonic stochastic resonance

The spatiotemporal SR in the  $\varphi^4$  model has been considered in a very interesting paper [39]. Recently we introduced the concept of solitonic stochastic resonance (SSR) [40] where a soliton moves in a bistable potential created by space-dependent external forces driven by a periodic signal and noise. This seems to be equivalent to the conventional setup for SR, however the conditions for the existence of SSR are different from that of SR with a point

particle in a bistable potential. The situation for SSR can produce very interesting phenomena like the transformation of the soliton into a three-“particle” system of two solitons and an antisoliton [40].

Here we will present another framework for SSR.

The function

$$\phi(x, t) = \tanh \{B[x - x_0 - A \sin(\omega t) - Df(t)]\}, \quad (25)$$

where  $f(t)$  is defined in Eq. (24), can be used to find analytic solutions to nonlinear partial differential equations.

Recall that function (25) is a SR solution (see Eq. (23)). For instance, if we take the time-series produced by  $\phi(x=0, t)$  (with  $B = 12, A = 0.67, \omega = 0.88, x_0 = 2$ , and  $f(t)$  is the function (24)) we obtain a new kind of SSR from (25). In fact, using the solution (25) we can prove that the overdamped perturbed  $\varphi^4$  equation

$$\phi_t - \phi_{xx} - B^2(\phi - \phi^3) = \frac{B[\omega A \cos(\omega t) + D\dot{f}(t)]}{\cosh^2[B(x - x_0)]} + F(x), \quad (26)$$

where  $F(x) = a \tanh[B(x - x_0)]$ , possesses a different kind of SSR.

We can calculate analytically the SNR for the dynamics of equation (26).

Suppose that, in equation (26), instead of  $f(t)$ , the noise is described by the function  $h(t) = (2/\pi) \arcsin f(t)$ , and  $f(t)$  is given by function (24). This is equivalent to a uniformly distributed noise in the interval  $(0, 1)$ . We will define  $b/2 = x_0 - A$ .

Following the ideas of Ref. [34], we can calculate an approximate analytical expression for the SNR when  $B \gg 1$ :

$$SNR = \begin{cases} 0 & \text{for } \frac{D}{2} < \frac{b}{2} - A \\ \frac{1}{D}(\frac{D}{2} - \frac{1}{2} + 2A) & \text{for } \frac{b}{2} - A \leq \frac{D}{2} \leq \frac{b}{2} + A \\ \frac{2A}{D} & \text{for } \frac{D}{2} > \frac{b}{2} + A \end{cases}$$

It is evident that there is a maximum in the curve SNR(D).

Our theoretical results on the theory of solitons perturbed by external forces [42–45] allow us to understand the dynamics of Eq. (26) and to interpret the physics of solution

(25). In order to obtain the desired dynamics we should solve equation (26) with an initial condition representing a soliton situated in a vicinity of point  $x = x_0$ . In this case, the soliton center of mass will be oscillating inside the potential well created by the force  $F(x)$ . This is exactly what represents solution (25).

When we investigate the time-series obtained after the numerical simulation of Eq. (26), we obtain SSR as predicted by the theoretical solution (25).

The SNR vs  $D$  plot depends on the value of  $B$ . For very large values of  $B$ , the SNR vs  $D$  plot has a very nice maximum (see Fig. 13). The  $SNR(D)$  dependence shown in Fig. 13 was calculated numerically from the time-series generated by the function  $\phi(x = 0, t)$  as a solution of Eq. (26). The same result is obtained if we investigate the analytic solution (25). For very small values of  $B$ , the SSR disappears. Thus, this is a SSR that depends on the shape of the soliton. In particular, it depends on the width of the soliton, which can be expressed as  $S = 1/B$ . This SSR is different from the one obtained for a soliton moving in a bistable potential well [40] and that described in [39].

In Ref. [39] the synchronization of a linearly coupled chain of  $N$  overdamped bistable elements, subject to a deterministic periodic signal and uncorrelated white noise, is addressed in the continuous limit of a  $\varphi^4$  theory. The cooperation between noise and coupling is shown to lead to spatiotemporal stochastic resonance. There, the bistability of the  $\varphi^4$  equation on the potential  $U(\varphi) \sim (\varphi^2 - 1)^2$  plays the most important role. On the other hand, in our previous paper [40] we considered the stochastic resonance of a soliton moving in a bistable potential created by inhomogeneous external forces  $F(x)$ . In this paper, the output signal is the coordinate of the soliton center-of-mass. In the present work, the relevant output signal is  $\phi(x = 0, t)$ . The soliton is moving in a monostable well potential created by inhomogeneous external forces. However, the most striking feature is that the width of the soliton determines the existence or not of the solitonic stochastic resonance. The shape of the output signal possesses patterns that are very different from that obtained in a bistable system. They are more similar to the patterns that appear in threshold systems.

#### D. Patterns in the output signal of SR systems

Once we have an explicit solution that describes the stochastic resonance system as the following:

$$I(t) = g(P(t) + \eta(t)) \quad (27)$$

and

$$I(t) = g(P(t) + \eta(t)) + \xi(t), \quad (28)$$

where  $P(t)$  is a periodic function,  $\eta(t)$  and  $\xi(t)$  are different manifestations of noise dynamics, we can calculate the SNR exactly. We should note that SNR is the main measure of stochastic resonance and is widely used in SR literature.

For instance, let us define the different noises as follows.  $\xi(t)$  is a white noise with zero mean and correlation function:

$$\langle \xi(t)\xi(t + \tau) \rangle = Q\delta(\tau) \quad (29)$$

where  $Q$  is a constant parameter.  $\eta(t)$  is a Gaussian noise with zero mean and correlation function:

$$\langle \eta(t)\eta(t + \tau) \rangle = \sigma^2 \exp(-\tau/\tau_F) \quad (30)$$

Following Ref. [38] we can consider the case

$$g(V) = V^3, \quad (31)$$

where

$$V = \alpha \sin(w_0 t) + \eta(t) \quad (32)$$

In this case the SNR is:

$$SNR = \pi \frac{18\alpha^2\sigma^4 + 9\alpha^4\sigma^2 + (9/8)\alpha^6}{2Q + \tau_F(44\sigma^6 + 54\alpha^2\sigma^4 + (27/2)\alpha^4\sigma^2)}. \quad (33)$$

This is exactly the SNR obtained in Ref. [38].

The static character of the present nonlinearities allows a direct statistical analysis, in which all quantities relevant to characterize the SNR in the output signal can be obtained from statistics computed directly on the input noises. In fact the SNR is a statistical measure based on the statistical properties of noises  $\eta(t)$  and  $\xi(t)$ .

Nevertheless, we believe that using our explicit functions we can obtain much more information about the output signal. Some of this information can have statistical character, but we will have also dynamical and geometrical information about the output signal.

For instance, we can predict the values of the local maxima and minima in the time-series, and the distance between them. We can obtain the exact analytical shape of the extrema.

In any stochastic resonance output signal there are patterns. These patterns can be different for different systems. The following function

$$I_n = \frac{\tanh[B(A \sin(\omega n) + D \cos(\theta \pi z^n)) - V_{th}] + 1}{2} \quad (34)$$

is the analytical solution for a circuit with  $I - V$  characteristic of type:

$$g(V) = \begin{cases} 0 & \text{for } V < V_{th} \\ 1 & \text{for } V > V_{th} \end{cases}$$

(see Ref. [36]). A typical time-series is shown in Fig. 14a.

In Fig. 14b it is shown the typical time-series for

$$g(V) = \begin{cases} -1 & \text{for } V < -0.5 \\ 0 & \text{for } -0.5 \leq V \leq 0.5 \\ 1 & \text{for } V > 0.5 \end{cases} \quad (35)$$

In Fig. 14c we show the function

$$I_n = \left( \frac{\tanh(BV_n) + 1}{2} \right) bV_n, \quad (36)$$

where

$$V_n = A \sin(\omega n) + D \cos(\theta \pi z^n), \quad (37)$$

which is the output signal for a circuit system with the characteristic

$$g(V) = \begin{cases} 0 & \text{for } V < V_{th} \\ b(V - V_{th}) & \text{for } V > V_{th} \end{cases}. \quad (38)$$

Fig. 14d shows the output signal

$$I_n = g(V_n) + \xi_n, \quad (39)$$

where  $g(V) = V^3$ ,  $V_n = \alpha \sin(\omega n) + \eta_n$ ,  $\eta_n = DY_n$ ,  $Y_n = \ln\left(\frac{X_n}{1-X_n}\right)$ ,  $X_n = \sin^2(\theta\pi z^n)$ ,  $\xi_n = Q \ln\frac{Z_n}{1-Z_n}$ , and  $Z_n = \sin^2(\theta\pi\pi^n)$ .

All these systems present stochastic resonance. All these systems can be tuned to have the same SNR. However, note that all the patterns are different. Compare them to the typical time-series of a classic bistable stochastic resonance system shown in Fig. 15. The information about these patterns is in the explicit functions that can be written down using our stochastic functions.

We can even make predictions about the outcomes in these stochastic systems. For instance, in the function (34) we can say that with a probability  $p = 0.8$ , after the function  $I_n$  has taken the value  $I_n = 1$ , it will take the value  $I_n = 0$ . Meanwhile, we can expect that it will remain in the state  $I_n = 0$  for an average time approximately equal to the period of the periodic input signal.

On the other hand, the output function (36) will give us much more information about the actual shape of the input periodic signal than the functions (34) and (35).

Systems with intrinsic and external noises are expected to be very random. Nevertheless, using the theoretical information obtained from our explicit function (39), we can make very remarkable predictions. For instance, if the output signal takes a “large” negative value (say  $I_n = -20$ ), then with absolute certainty we can predict that the next values will be negative and  $|I_n| \rightarrow 0$ . When  $I_n$  reaches the value  $I_n = 0$ , we can predict that the next value will be positive, but the exact value is unpredictable. When it takes this positive value, the next value will be negative with absolute certainty. The larger the absolute value of  $I_n$  when it takes a positive value, the larger the absolute value of the next negative value that it

will take. Note that all the randomness of this dynamics is produced when  $I_n$  is near zero. When  $I_n$  is far from zero, we can make exact predictions of the next values. All this can be corroborated when we observe the first-return map of this dynamics (Fig. 16).

We can see the stochastic resonance as a phenomenon that transforms a complex dynamics into a simpler one. That is, the output signal is less complex than the input signal. But there are also phenomena that lead to a more complex behavior (e.g. the chaotic systems).

Using our functions we can predict the existence of new complex phenomena.

After an analysis of the functions  $X_n = \sin^2(\theta\pi z^n)$ , which we have shown to produce complex dynamics, the first characteristics that surface are the following: the function can be re-written in the form  $X_n = h(f(n))$ , where the argument function  $f(n)$  grows exponentially and the function  $h(y)$  is always finite and periodic.

However, a more deep analysis shows that (to produce complex behavior) the function  $f(n)$  has not to be exponential all the time, and function  $h(y)$  has not to be periodic.

In fact, it is sufficient that the function  $f(n)$  be a nonperiodic oscillating function where there are repeating intervals with finite exponential behavior. For instance, this can be a chaotic function. On the other hand, function  $h(y)$  should be noninvertible. In other words, it should have different maxima and minima. The inverse “function” of  $h(y)$  should be multivalued.

The complexity of the output dynamics is proportional to the number of extrema of function  $h(y)$ .

For example, the following system can produce a dynamics similar to that obtained with our function  $X_n = \sin^2(\theta\pi z^n)$ :

$$X_{n+1} = \begin{cases} aX_n, & \text{if } X_n < Q \\ bY_n, & \text{if } X_n > Q \end{cases} \quad (40)$$

$$Y_{n+1} = \sin^2(d \arcsin \sqrt{Y_n}) \quad (41)$$

$$Z_{n+1} = g(X_n) \quad (42)$$

where  $g(X_n)$  is a function with several maxima and minima. The first return map is shown in Fig. 17. In fact, this is a completely new chaotic phenomenon because the dynamics is completely unpredictable. So, when the input is a simple chaotic signal and the system is an electronic circuit with the  $I - V$  characteristic shown in Fig. 15a, then we will have a very complex output. This phenomenon is the opposite to the stochastic resonance. Compare two  $I - V$  characteristic curves for a phenomenon that simplifies the dynamics and for a new phenomenon that makes the dynamics extremely complex in Fig. 18. In Ref. [46] a theory of nonlinear circuits is presented. There we can find different methods to construct circuits with these  $I - V$  characteristic curves.

All the results presented in subsection VI-D, which are related to the figures 14-18 were obtained through theoretical calculations.

### **E. Applications in real systems**

In this subsection we will present some examples that show how our technique can be used in real world applications.

Our group have designed and constructed a nonlinear circuit (using a concave resistor) with the I-V characteristic described by equation (36) (see Ref. [46]). We wished to check our theoretical results about the dependence of SNR on the Lyapunov exponent of the chaotic noise. We also desired to observe the patterns for the output signal predicted by our theory.

In order to have different driving chaotic signals, we produced numerical time-series using the exactly solvable map (3) for different  $z$ .

Then, we transformed the numerical time-series into analog signals using a converter. These analog signals plus a subthreshold periodic signal were introduced as the voltage to the concave resistor circuit. The current in the concave resistor was taken as the output signal.

We should say that the amplification of the SNR in the interval  $\ln(3/2) < \lambda < \ln 2$  was clearly observed. The maximum SNR for  $\lambda = \ln(3/2)$  was 5 times larger than for  $\lambda \geq 3$  or

for any random noise.

We will present further details of these experiments elsewhere.

Thus, in the case that SR is used for the amplification of small signals (as in the dithering effect) such that the added external noise is a controllable and manipulable parameter, our recommendation is to utilize a uniform chaotic noise with a Lyapunov exponent of the order of  $\lambda \approx \ln(3/2)$ .

Using the techniques described in Ref. [46] it is possible to construct nonlinear circuits with the I-V characteristics shown in Fig. 18.

For our experiments we used the twin-transistor circuit [46].

As an input signal (voltage), we introduced an analog chaotic signal previously produced by a nonlinear map.

Playing with different parameters we were able to produce different unpredictable dynamics very similar to those obtained from our function (2) and the figures 2-3. The same results can be obtained when we take the input signal from a chaotic electronic circuit.

In general, the patterns or absence of patterns (it depends on the nonlinearity) predicted by our theory are completely confirmed by the experiments.

Some of these experiments are complicated and should be explained in a separate paper.

In many relevant applications it is important to get resonances or (in other cases) to avoid resonances.

Recently a new resonance concept was introduced: the geometrical resonance [48,40].

In the usual linear resonance phenomena, the amplitude and frequency of the driving force are the most important characteristics. However, in nonlinear systems the shape of the driving signal becomes crucial. The geometrical resonance considers the amplitude, the frequency, and the shape of the perturbation.

Suppose we have a nonlinear system  $A$  which for some application should be driven by a specific driving signal with a given shape. In that case, we can use the output signal of another system  $B$  as the input signal of the system  $A$ . So it is important to predict the shape of the output of nonlinear systems. With such information we can design the appropriate

system to produce the desired signal needed for the driving of the system  $A$ .

In subsection VI-D we have shown that we can predict specific patterns and the shape of the output signal of nonlinear stochastic systems. This is a step forward in the control of chaotic and stochastic systems.

In general, it is very important to find patterns and regularities in the stochastic dynamical systems. In fact, not everything that can be observed can be predicted, only the regularities in the observations are the “province of science” [47].

There are many stochastic systems (including systems presenting stochastic resonance) where predictions are crucial. In this case we mean predictions of the true values of the outcomes using the previous values. Among the concerned areas are the following: geophysics, meteorology, climatology, social sciences, etc. [49–52]

In subsection VI-D we have investigated a system with external noise and intrinsic noise. These noisy perturbations are very unpredictable functions. However, we have shown theoretically that we are able to make direct predictions of the time-series outcomes. There are many systems with this behavior [38]. When we observe the Fig. 14d, we note that there are very remarkable bursts in the time-series. In all the mentioned applications it is very important to predict these bursts. We have shown that we can do this.

## VII. CONCLUSION

In conclusion, we can construct functions that are exact solutions to chaotic dynamical systems. Moreover, we have generalized functions that cannot be generated by a finite recursive algorithm. They can be utilized as theoretical paradigms of stochastic processes. Considering the fact that these are explicit functions, we can use them to solve (analytically) many theoretical problems in stochastic dynamical systems. Thus, we can apply dynamical concepts to describe processes that are usually considered only statistically [28].

## VIII. ACKNOWLEDGEMENT

Eng. José Juan Suárez (UNEXPO, Venezuela) and Dr. Gustavo Gutiérrez (USB, Venezuela) have collaborated in the design and construction of the nonlinear circuits.

---

- [1] A. M. Ferrenberg, D. P. Landau, and Y. J. Wong, *Phys. Rev. Lett.* **69**, 3382 (1992).
- [2] R. M. D'Souza, Y. Bar-Yam, and M. Kardar, *Phys. Rev. E* **57**, 5044 (1998).
- [3] J. Nogués, J. L. Costa-Krämer, and K. V. Rao, *Physica A* **250**, 327(1998); M. E. Fisher, *Physica A* **263**, 554 (1999).
- [4] F. James, *Comp. Phys. Commun.* **60**, 329 (1990); *Chaos, Solitons and Fractals* **6**, 221 (1995).
- [5] L. Yu, E. Ott, and O. Chen, *Phys. Rev. Lett.* **65**, 2935 (1990).
- [6] G. Paladin, M. Serva, and A. Vulpiani, *Phys. Rev. Lett.* **74**, 66 (1995).
- [7] V. Loreto, G. Paladin, and A. Vulpiani, *Phys. Rev. E* **53**, 2087 (1996).
- [8] G. Sugihara and R. M. May, *Nature* **344**, 734 (1990).
- [9] D. J. Wales, *Nature* **350**, 485 (1991).
- [10] A.A. Tsonis and J. B. Elsner, *Nature* **358**, 217 (1992).
- [11] S. M. Ulam, *A Collection of Mathematical Problems* (Interscience, New York, 1960).
- [12] P. Stein and S. M. Ulam, *Rozprawy Matematyczne* **39**, 401 (1964).
- [13] S. Katsura and W. Fukuda, *Physica A* **130**, 597 (1985).
- [14] S. Kawamoto and T. Tsubata, *J. Phys. Soc. Jpn.* **65**, 3078 (1996).
- [15] R. Brown and L. O. Chua, *Int. J. Bifurcation and Chaos* **6**, 219 (1996).
- [16] K. Umeno, *Phys. Rev. E* **55**, 5280 (1997).

- [17] J. A. González and L. B. Carvalho, *Mod. Phys. Lett. B* **11**, 521 (1997).
- [18] H. N. Nazareno, J. A. González, and I. Costa, *Phys. Rev. B* **57**, 13583 (1998).
- [19] J. A. González and R. Pino, *Comp. Phys. Comun.* **120**, 109 (1999).
- [20] J. P. Eckmann and D. Ruelle, *Rev. Mod. Phys.* **57**, 617 (1985).
- [21] S. Pincus and B. S. Singer, *Proc. Natl. Acad. Sci. USA* **93**, 2083 (1996).
- [22] R. Benzi, A. Sutera, and A. Vulpiani, *J. Phys. A* **14**, L453 (1981).
- [23] B. McNamara and K. Wiesenfeld, *Phys. Rev. A* **39**, 4859 (1989).
- [24] A. R. Bulsara and L. Gammaitoni, *Physics Today* **49**, 39 (1996).
- [25] L. Gammaitoni, P. Hänggi, P. Jung, and F. Marchesoni, *Rev. Mod. Phys.* **70**, 223 (1998).
- [26] K. Wiesenfeld and F. Moss, *Nature* **373**, 33 (1995).
- [27] E. Ippen, J. Lindner, and W. Ditto, *J. Stat. Phys.* **70**, 148 (1993).
- [28] T. L. Carroll and L. M. Pecora, *Phys. Rev. Lett.* **70**, 576 (1993).
- [29] T. Kapitaniak, *Phys. Rev. E* **49**, 5855 (1994).
- [30] W. Yang, M. Ding, and G. Hu, *Phys. Rev. Lett.* **74**, 3955 (1995).
- [31] A. Crisanti, M. Falcioni, G. Paladin, and A. Vulpiani, *J. Phys. A* **27**, L597 (1994).
- [32] V. S. Anishchenko, A. B. Neimann, and M. A. Safonova, *J. Stat. Phys.* **70**, 183 (1993).
- [33] P. Hänggi, P. Jung, C. Zerbe, and F. Moss, *J. Stat. Phys.* **70**, 25 (1993).
- [34] L. Gammaitoni, *Phys. Rev. E* **52**, 4691 (1995).
- [35] Z. Gingl, L. B. Kiss, and F. Moss, *Europhys. Lett.* **29**, 191 (1995).
- [36] F. Chapeau-Blondeau and K. Godivier, *Phys. Rev. E* **55**, 1478 (1997).
- [37] S. M. Bezrukov and I. Vodyanoy, *Nature* **385**, 319 (1997).

- [38] J. M. G. Vilar, G. Gomila, and J. M. Rubí, *Phys. Rev. Lett.* **81**, 14 (1998).
- [39] F. Marchesoni, L. Gammaitoni, and A. R. Bulsara, *Phys. Rev. Lett.* **76**, 2609 (1996).
- [40] J. A. González, B. A. Mello, L. I. Reyes, and L. E. Guerrero, *Phys. Rev. Lett.* **80**, 1361 (1998).
- [41] A. Witt, A. Neiman, and J. Kurth, *Phys. Rev. E* **55**, 5050 (1997).
- [42] J. A. González and J. A. Hołyst, *Phys. Rev. B* **45**, 10338 (1992).
- [43] J. A. González and B. A. Mello, *Phys. Scr.* **54**, 14 (1996).
- [44] J. A. González, L. E. Guerrero, and A. Bellorín, *Phys. Rev. E* **54**, 1265 (1996).
- [45] J. A. González, A. Bellorín, and L. E. Guerrero, *Phys. Rev. E* **60**, R37 (1999).
- [46] L. O. Chua, C. A. Desoer, and E. S. Kuh, *Linear and Nonlinear Circuits* (McGraw-Hill, New York, 1987).
- [47] J. B. Hartle, *Complexity* **3**, 22 (1997).
- [48] R. Chacón, *Phys. Rev. Lett.* **77**, 482 (1996).
- [49] L. Stone, P. I. Saporin, A. Huppert, and C. Price, *Geophys. Res. Lett.* **25**, 175 (1998).
- [50] B. Saltzman, H. Hu, and R. J. Oglesby, *Dynamics of Atmospheres and Oceans* **27**, 619 (1997).
- [51] H-S. Liu and B. F. Chao, *J. Atmos. Sci.* **55**, 227 (1998).
- [52] P. Babinec, *Phys. Lett A.* **225**, 179 (1997).

TABLE I. Representation of the matrix  $X_n^k$  given by Eq. (5) with  $z = 2$  and  $\theta_0 = 2^{1/2} - 1$ . Note that if we start with the same initial conditions, then we will have the same chaotic sequences

	$\theta_0$	$\theta_0 + 1$	$\theta_0 + 2$	$\theta_0 + 3$	$\theta_0 + 4$	$\theta_0 + 5$	$\theta_0 + 6$	$\theta_0 + 7$	$\theta_0 + 8$	$\theta_0 + 9$	$\theta_0 + 10$	$\theta_0 + 11$	$\theta_0 + 12$
$X_0$	0.9291	0.9291	0.9291	0.9291	0.9291	0.9291	0.9291	0.9291	0.9291	0.9291	0.9291	0.9291	0.9291
$X_1$	0.2634	0.2634	0.2634	0.2634	0.2634	0.2634	0.2634	0.2634	0.2634	0.2634	0.2634	0.2634	0.2634
$X_2$	0.7762	0.7762	0.7762	0.7762	0.7762	0.7762	0.7762	0.7762	0.7762	0.7762	0.7762	0.7762	0.7762
$X_3$	0.6948	0.6948	0.6948	0.6948	0.6948	0.6948	0.6948	0.6948	0.6948	0.6948	0.6948	0.6948	0.6948
$X_4$	0.8481	0.8481	0.8481	0.8481	0.8481	0.8481	0.8481	0.8481	0.8481	0.8481	0.8481	0.8481	0.8481
$X_5$	0.5151	0.5151	0.5151	0.5151	0.5151	0.5151	0.5151	0.5151	0.5151	0.5151	0.5151	0.5151	0.5151
$X_6$	0.9990	0.9990	0.9990	0.9990	0.9990	0.9990	0.9990	0.9990	0.9990	0.9990	0.9990	0.9990	0.9990
$X_7$	0.0036	0.0036	0.0036	0.0036	0.0036	0.0036	0.0036	0.0036	0.0036	0.0036	0.0036	0.0036	0.0036
$X_8$	0.0146	0.0146	0.0146	0.0146	0.0146	0.0146	0.0146	0.0146	0.0146	0.0146	0.0146	0.0146	0.0146
$X_9$	0.0578	0.0578	0.0578	0.0578	0.0578	0.0578	0.0578	0.0578	0.0578	0.0578	0.0578	0.0578	0.0578
$X_{10}$	0.2181	0.2181	0.2181	0.2181	0.2181	0.2181	0.2181	0.2181	0.2181	0.2181	0.2181	0.2181	0.2181

TABLE II. Representation of the matrix  $X_n^k$  defined by Eq. (5) with  $z = 3/2$  and  $\theta_0 = 1$ . Note that all the column-sequences possess the same initial conditions  $x_0 = 0$ . However, all the sequences are different in general.

	$\theta_0$	$\theta_0 + 1$	$\theta_0 + 2$	$\theta_0 + 3$	$\theta_0 + 4$	$\theta_0 + 5$	$\theta_0 + 6$	$\theta_0 + 7$	$\theta_0 + 8$	$\theta_0 + 9$	$\theta_0 + 10$	$\theta_0 + 11$	$\theta_0 + 12$
$X_0$	0	0	0	0	0	0	0	0	0	0	0	0	0
$X_1$	1	0	1	0	1	0	1	0	1	0	1	0	1
$X_2$	1/2	1	1/2	0	1/2	1	1/2	0	1/2	1	1/2	0	1/2
$X_3$	0.8535	1/2	0.1464	1	0.1464	1/2	0.8535	0	0.8535	1/2	0.1464	1	0.1464
$X_4$	0.0380	0.1464	0.3086	1/2	0.6913	0.8535	0.9619	1	0.9619	0.8535	0.6913	1/2	0.3086
$X_5$	0.9157	0.3086	0.4024	0.8535	0.0096	0.9619	0.2222	1/2	0.7777	0.0380	0.9903	0.1464	0.5975
$X_6$	0.8865	0.4024	0.2643	0.9619	0.0215	0.7777	0.5490	0.1464	0.9975	0.0842	0.6451	0.6913	0.0590
$X_7$	0.0711	0.2643	0.5245	0.7777	0.9519	0.9975	0.9016	0.6913	0.4266	0.1828	0.0292	0.0096	0.1295
$X_8$	0.8447	0.5245	0.1213	0.9975	0.1923	0.4266	0.9087	0.0096	0.7674	0.6214	0.0649	0.9784	0.2751
$X_9$	0.9686	0.1213	0.7410	0.4266	0.3964	0.7674	0.1020	0.9784	0.0009	0.9571	0.1421	0.7137	0.4571
$X_{10}$	0.7544	0.7410	0.0002	0.7674	0.7275	0.0009	0.7803	0.7137	0.0021	0.7928	0.6998	0.0037	0.8051

TABLE III. Representation of the matrix  $X_n^k$  defined by Eq. (5) with  $z = 4/3$  and  $\theta_0 = 1/6$ . Note that the horizontal row-sequences possess periods  $3^n$ . All the next-values in the column-sequences are unpredictable.

	$\theta_0$	$\theta_0 + 1$	$\theta_0 + 2$	$\theta_0 + 3$	$\theta_0 + 4$	$\theta_0 + 5$	$\theta_0 + 6$	$\theta_0 + 7$	$\theta_0 + 8$	$\theta_0 + 9$	$\theta_0 + 10$	$\theta_0 + 11$	$\theta_0 + 12$
$X_0$	1/4	1/4	1/4	1/4	1/4	1/4	1/4	1/4	1/4	1/4	1/4	1/4	1/4
$X_1$	0.4131	0.9698	0.1169	0.4131	0.9698	0.1169	0.4131	0.9698	0.1169	0.4131	0.9698	0.1169	0.4131
$X_2$	0.6434	0.0531	0.2014	0.8431	0.9177	0.3019	0.0134	0.5290	0.9966	0.6434	0.0531	0.2014	0.8431
$X_3$	0.8951	0.4515	0.1712	0.9996	0.1430	0.4903	0.8702	0.0015	0.8139	0.5676	0.0932	0.9906	0.2333
$X_4$	0.9929	0.6920	0.2118	0.0006	0.2556	0.7387	0.9989	0.7933	0.3138	0.0081	0.1616	0.6309	0.9780
$X_5$	0.6475	0.0675	0.1584	0.7792	0.9668	0.4302	0.0018	0.3463	0.9291	0.8462	0.2261	0.0308	0.5633
$X_6$	0.0393	0.9703	0.2695	0.3683	0.9239	0.0086	0.7980	0.5534	0.1235	0.9998	0.1420	0.5262	0.8194
$X_7$	0.4955	0.5309	0.4425	0.5837	0.3901	0.6355	0.3390	0.6858	0.2897	0.7340	0.2427	0.7796	0.1987
$X_8$	0.7550	0.7849	0.8132	0.8400	0.8651	0.8884	0.9097	0.9290	0.9461	0.9609	0.9735	0.9837	0.9914
$X_9$	0.4054	0.9858	0.1903	0.2718	0.9995	0.3124	0.1565	0.9733	0.4495	0.0686	0.9093	0.5907	0.0151
$X_{10}$	0.0160	0.6018	0.9938	0.4460	0.0008	0.5054	0.9996	0.5430	0.0045	0.4089	0.9866	0.6383	0.0267

TABLE IV. Representation of the matrix  $X_n^k$  given by Eq. (5) with  $z = \pi$  and  $\theta_0 = 1/4$ . Note that it is difficult even to find “clusters” of equal values in different column-sequences. All column-sequences are completely random and different.

	$\theta_0$	$\theta_0 + 1$	$\theta_0 + 2$	$\theta_0 + 3$	$\theta_0 + 4$	$\theta_0 + 5$	$\theta_0 + 6$	$\theta_0 + 7$	$\theta_0 + 8$	$\theta_0 + 9$	$\theta_0 + 10$	$\theta_0 + 11$	$\theta_0 + 12$
$X_0$	1/2	1/2	1/2	1/2	1/2	1/2	1/2	1/2	1/2	1/2	1/2	1/2	1/2
$X_1$	0.3897	0.0516	0.0457	0.3761	0.7983	0.9995	0.8307	0.4169	0.0646	0.0348	0.3494	0.7756	0.9976
$X_2$	0.9895	0.7599	0.3653	0.0562	0.0286	0.3002	0.6984	0.9708	0.9444	0.6359	0.2412	0.0107	0.0906
$X_3$	0.4950	0.4753	0.4556	0.4360	0.4165	0.3972	0.3780	0.3589	0.3401	0.3216	0.3033	0.2853	0.2677
$X_4$	0.7996	0.4643	0.2603	0.9388	0.0012	0.9002	0.3252	0.3937	0.8535	0.0114	0.9684	0.2003	0.5356
$X_5$	0.9997	0.9940	0.9807	0.9601	0.9324	0.8982	0.8579	0.8120	0.7615	0.7069	0.6492	0.5892	0.5278
$X_6$	0.7869	0.5423	0.1479	0.9978	0.0881	0.6342	0.7058	0.0498	0.9849	0.2060	0.4662	0.8458	0.0030
$X_7$	0.0521	0.8342	0.7685	0.0216	0.4881	0.9847	0.2517	0.1484	0.9368	0.6171	0.0003	0.6509	0.9186
$X_8$	0.1640	0.7578	0.3299	0.5757	0.5214	0.3822	0.7096	0.2064	0.8663	0.0746	0.9681	0.0066	0.9997
$X_9$	0.5777	0.8516	0.9930	0.9485	0.7348	0.4326	0.1558	0.0087	0.0469	0.2559	0.5569	0.8365	0.9891
$X_{10}$	0.0013	0.0343	0.1084	0.2171	0.3507	0.4976	0.6446	0.7789	0.8885	0.9639	0.9982	0.9885	0.9357

FIG. 1. One-valued first-return map produced by function (2) with  $z = 5$ .

FIG. 2. Multivalued first-return maps produced by function (2): (a)  $z = 3/2$ ; (b)  $z = 8/5$ .

FIG. 3. Random first-return maps for  $z = \pi$ : (a) first-return map produced by function (2); (b) first-return map produced by function (2) and with transformation  $Y_n = (2/\pi) \arcsin(X_n^{1/2})$ .

FIG. 4. Mean distance versus number of steps for a random walk generated with the random numbers  $Y_n = (2/\pi) \arcsin(X_n^{1/2})$ , where  $X_n$  is given by function (2).

FIG. 5. Predicted values one-step into the future vs observed values for the time-series generated by function (2) with  $z = e$ , after the transformation  $Y_n = (2/\pi) \arcsin(X_n^{1/2})$ .

FIG. 6. In the interval  $\ln(3/2) < \lambda < \ln 2$ , the maximum SNR is shifted to the right and is amplified.

FIG. 7. Function  $K(D)$  as given by equation (22). Solid line,  $z = 1.5$ ; dotted line,  $z = 2$ ; dashed line,  $z = 2.5$ ; dot-dashed line,  $z = 3$ . Note that as  $z$  is decreased, the minimum of function  $K(D)$  is deeper and is shifted to the right.

FIG. 8. Time-series and first-return maps generated by the noise-driven dynamical system (20). a) and d)  $D = 0.5$ ; b) and e)  $D = 2$ ; c) and f)  $D = 20$ . In all cases  $\varepsilon = 0.5$ ,  $\alpha = 1$ ,  $\delta = 0.3$ ,  $z = 1.5$

FIG. 9. Time-series generated by the noise-driven dynamical system (20). a)  $D = 2$ , b)  $D = 10$ . In all cases  $\varepsilon = 0.5$ ,  $\alpha = 1$ ,  $\delta = 0.1$ ,  $z = 1.1$ . Note that in case b) the control is so good that the output signal is almost periodic and is confined to a very narrow interval of values. Note also that in this case the noise intensity is 5 times larger!

FIG. 10. The explicit function (23) can behave as a stochastic resonance system. This figure shows the SNR vs noise intensity ( $D$ ) for  $B = 24$  and  $B = 1$ . Note that for  $B = 1$  there is no maximum in this plot.

FIG. 11. Chaotic time-series generated by the continuous function (24).

FIG. 12. SNR vs noise intensity ( $D$ ) for the dynamics of system (16). Here the “noise”  $\eta(t)$  is defined as  $\eta(t) = \ln [f(t)/(1 - f(t))]$ , where  $f(t)$  is given by (24).

FIG. 13. SNR vs noise intensity ( $D$ ) for the dynamics of system (26). The SNR is calculated from the time-series generated by the function  $\phi(x = 0, t)$ .

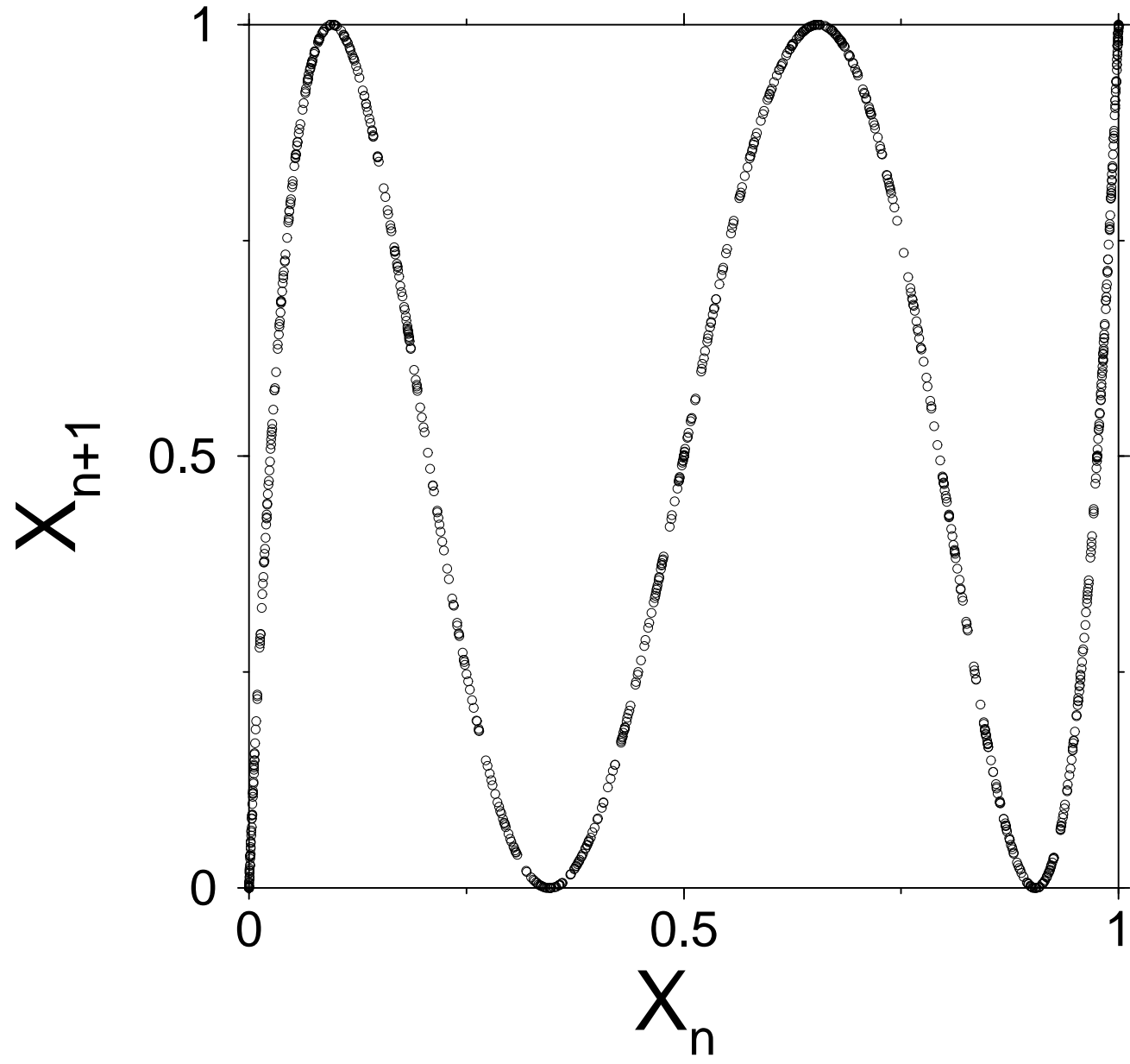
FIG. 14. Time series produced by explicit functions that describe different stochastic resonance systems. a) Function (34), b) System (35), c) Function (36), d) Function (39).

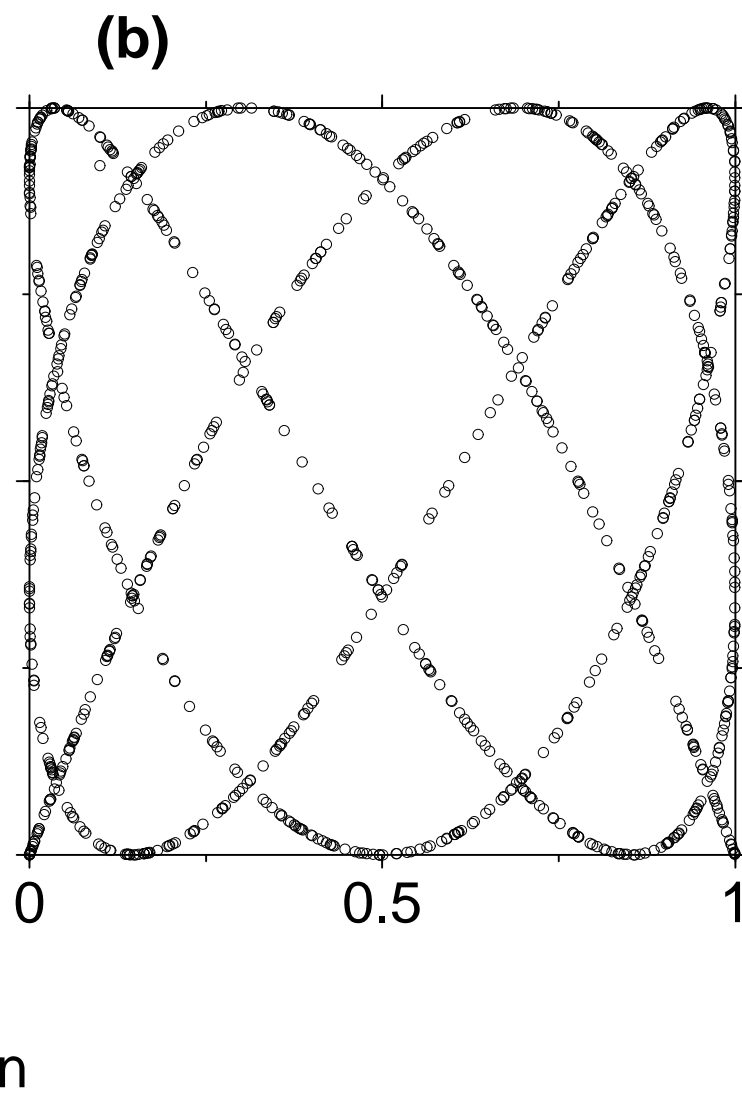
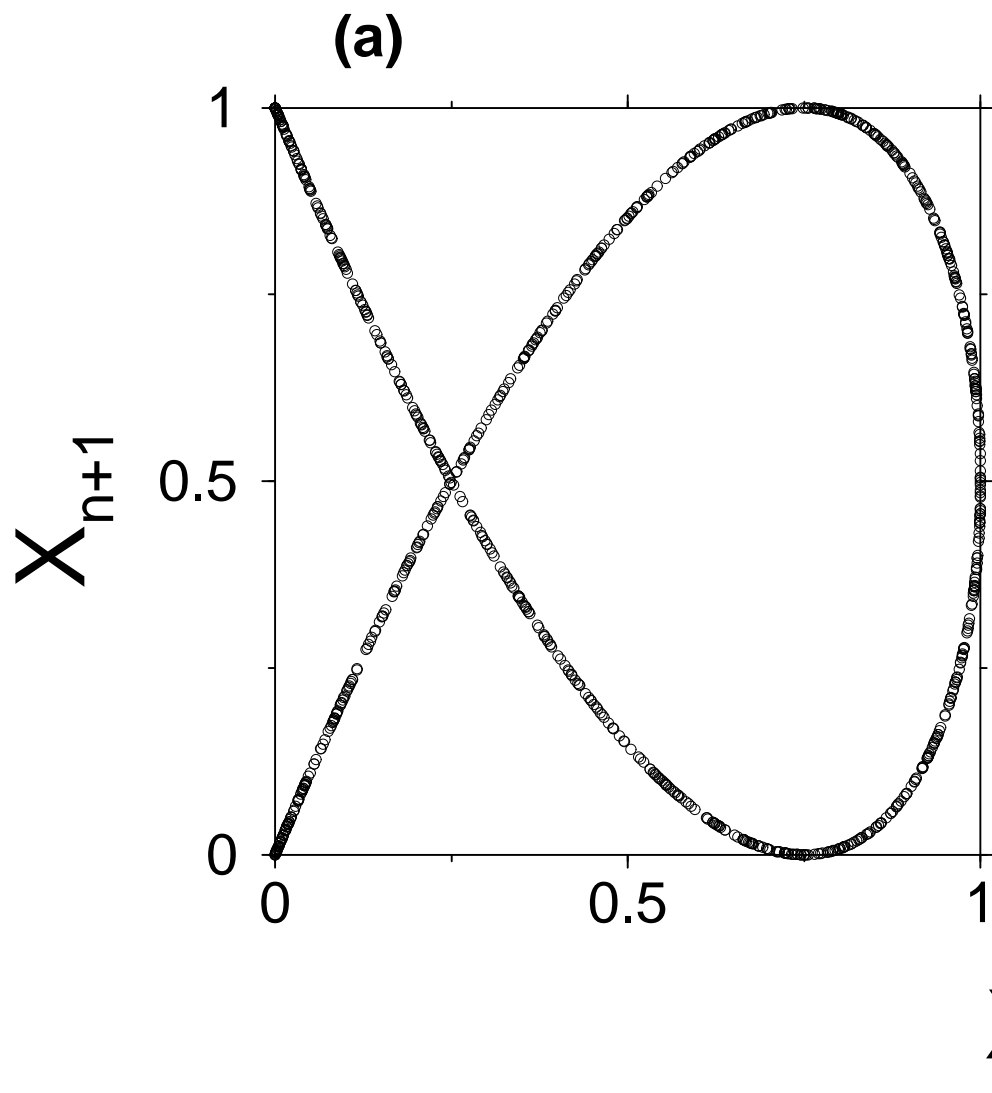
FIG. 15. Typical time series for a bistable stochastic resonance system as that described by equation (16).

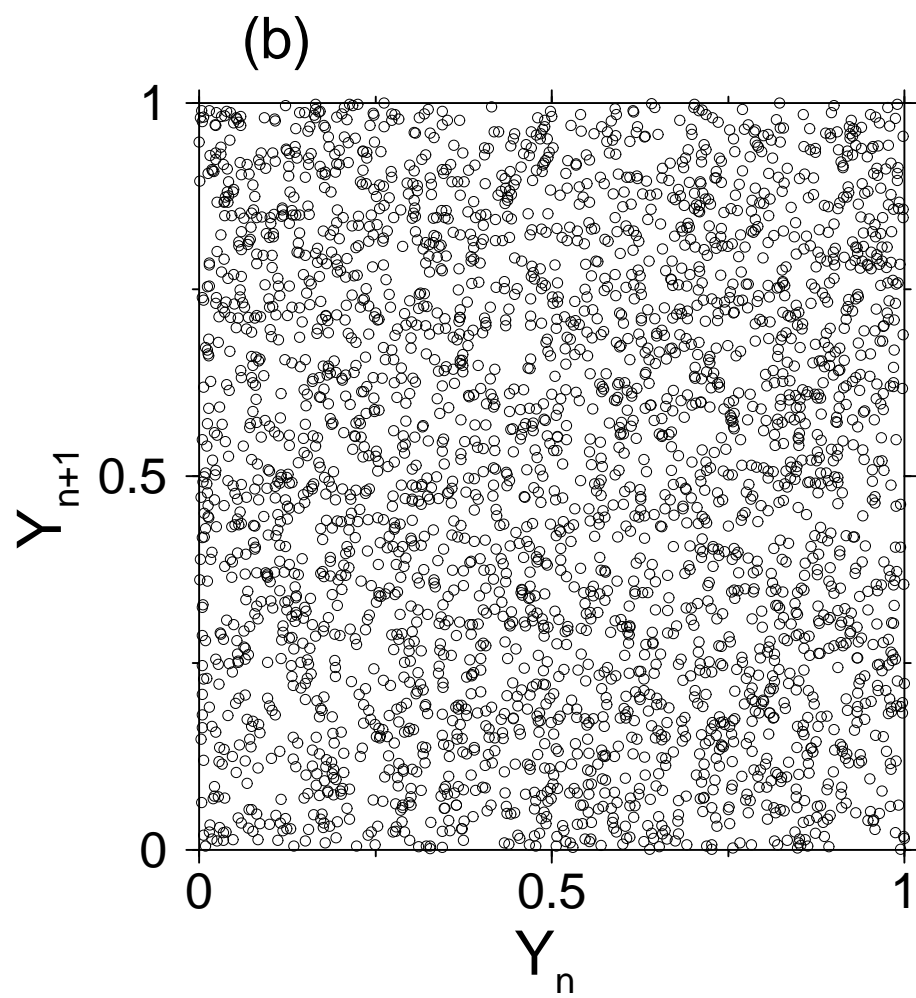
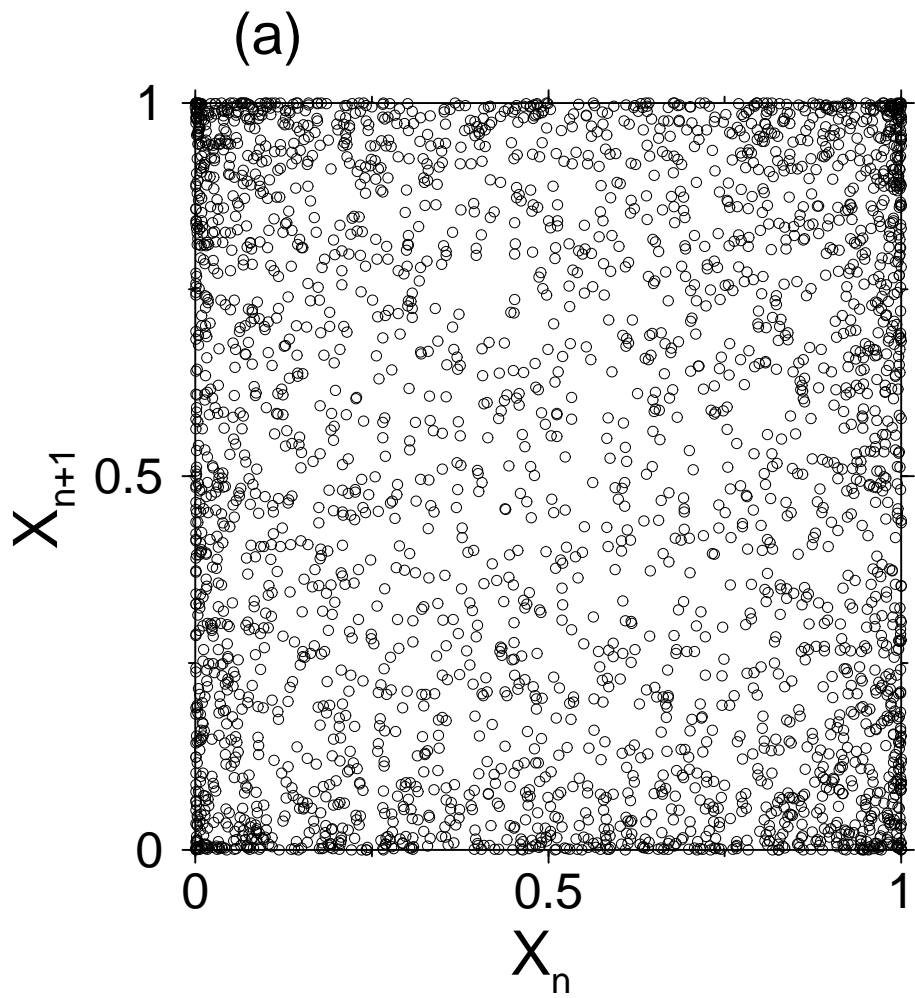
FIG. 16. First-return map produced by function (39), which describes a stochastic resonance system with intrinsic noise. a) Situation of stochastic resonance  $D = 0.16$ . b) Situation out of stochastic resonance  $D = 0.3$ .

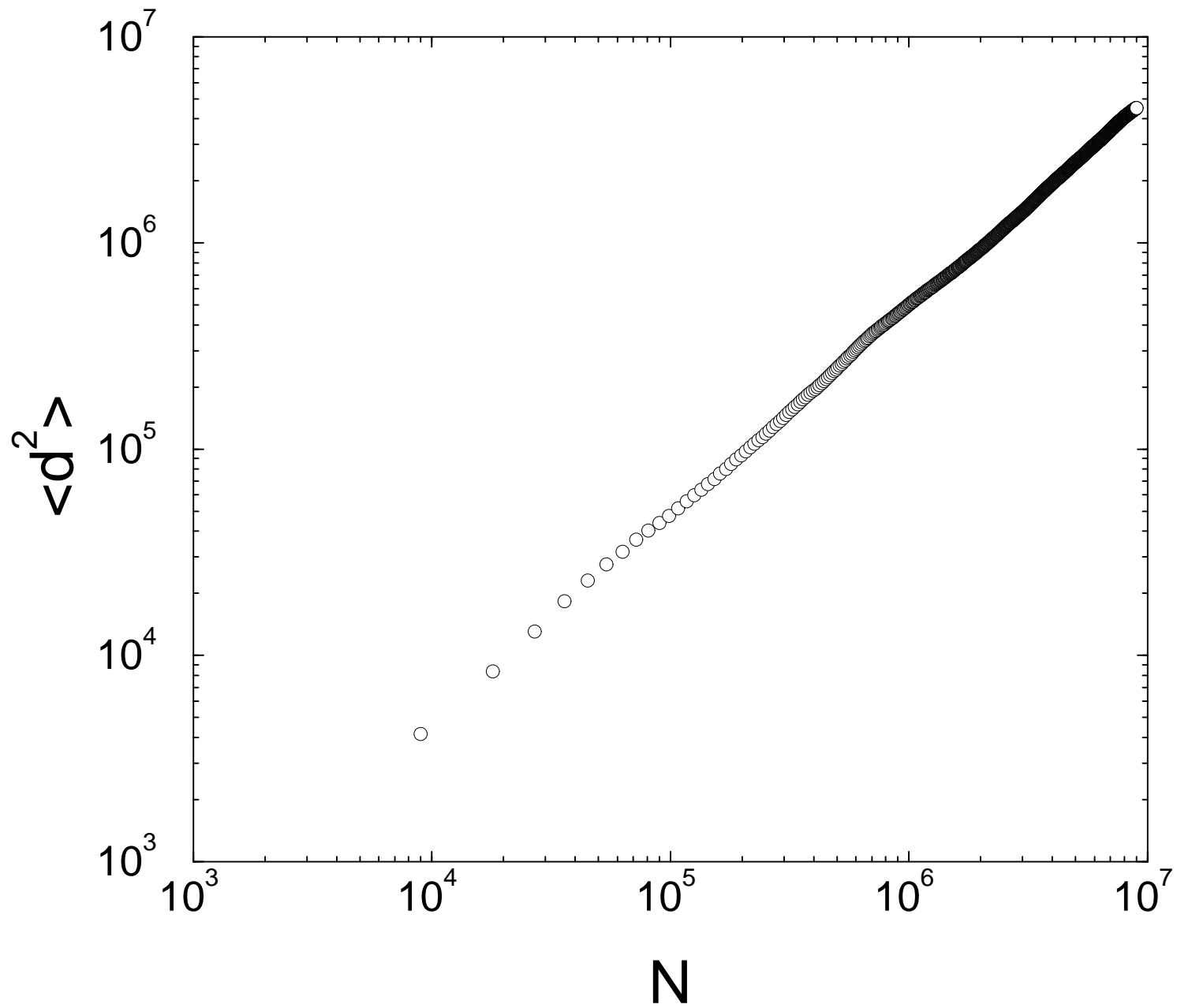
FIG. 17. First-return map produced by the dynamics of variable  $Z_n$  in the dynamical system (39-41). a) Function  $g(x)$  possesses 1 local extremum. b) Function  $g(x)$  possesses 100 local extremas.

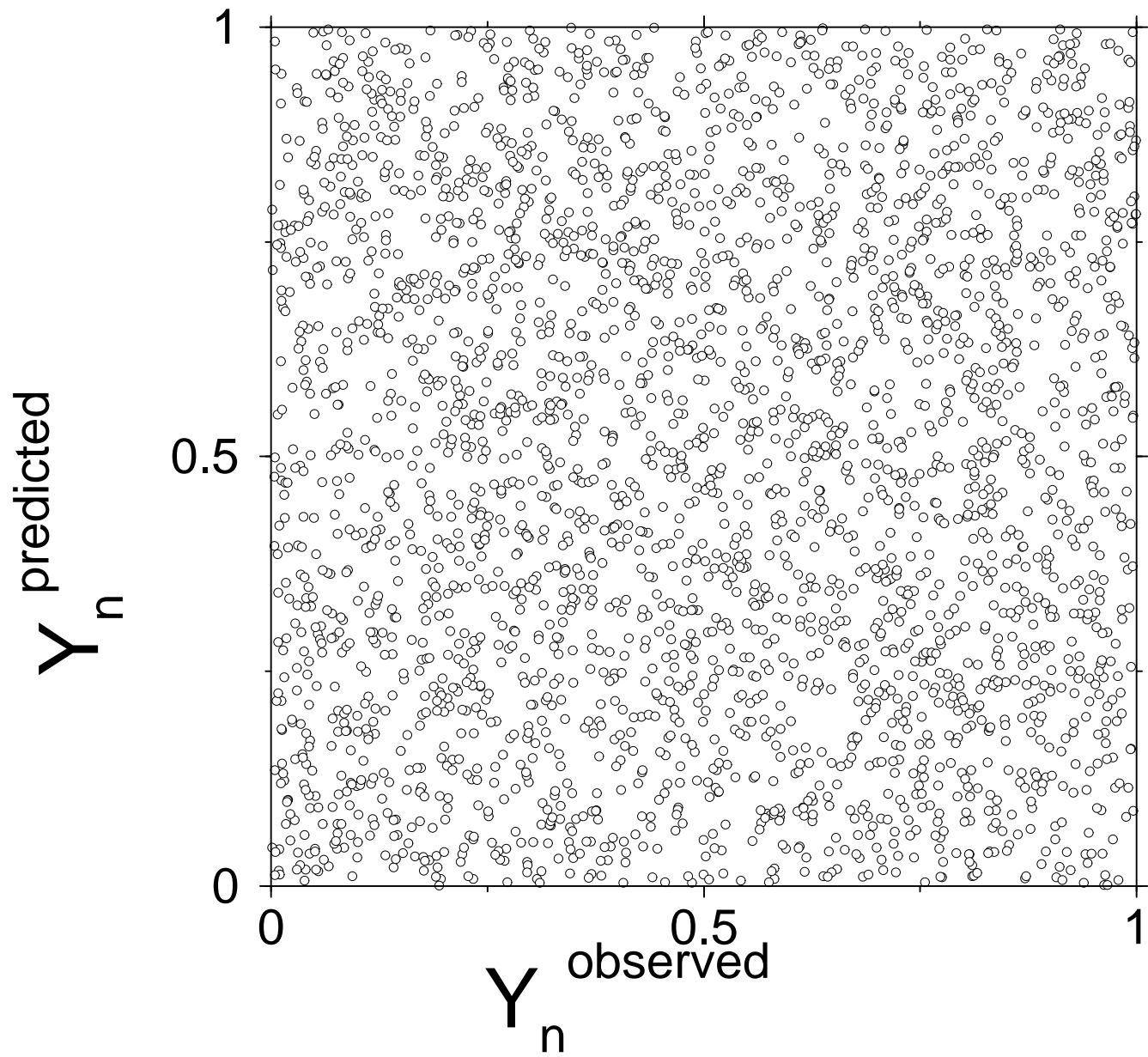
FIG. 18.  $I - V$  characteristic curves of two nonlinear circuits: a) With some appropriately chosen input signal, this circuit can produce a very complex output signal (see discussion in the text). b) If the input signal is composed of a periodic signal and noise, the output signal will be less complex than the input signal. In fact, this will be a stochastic resonance system.

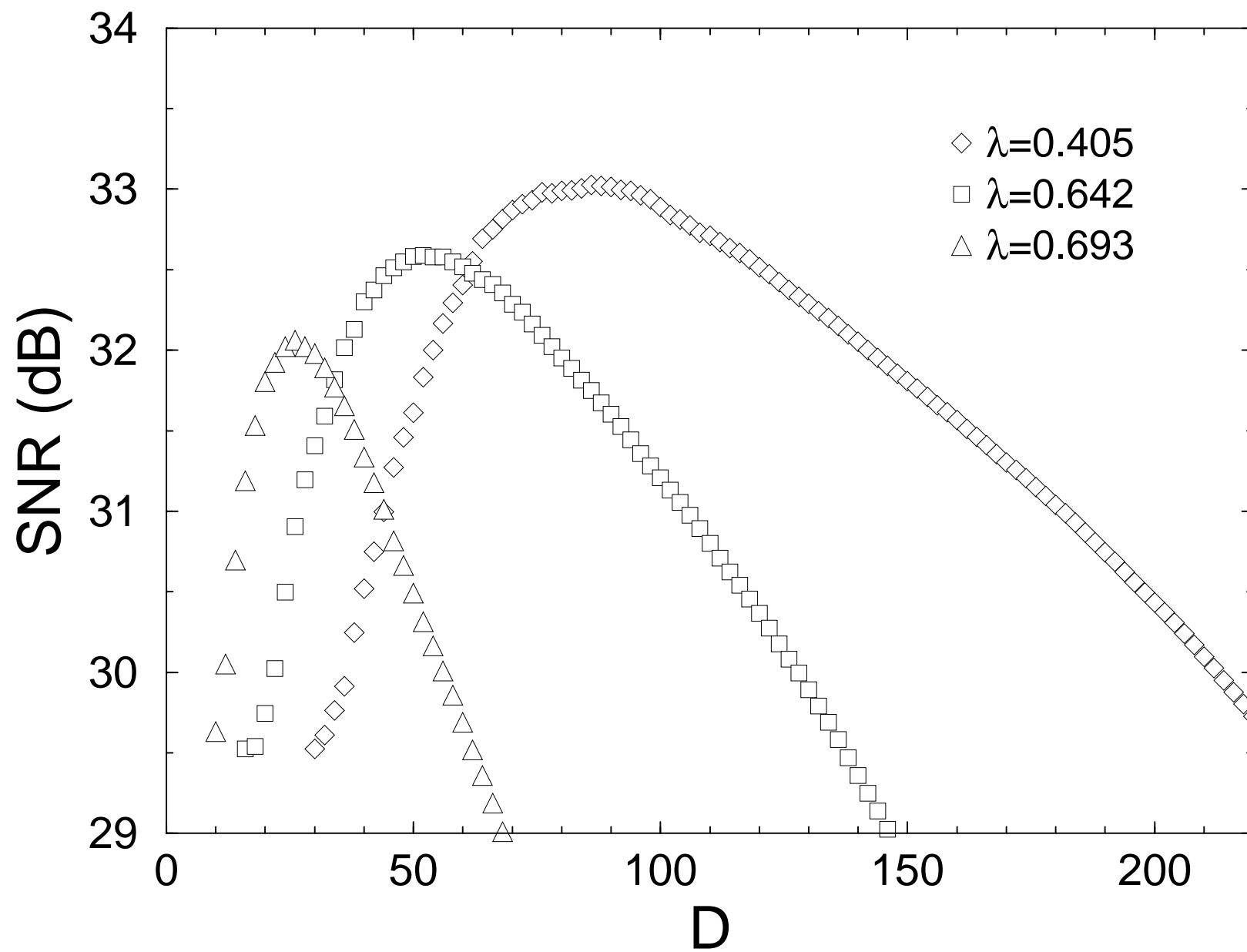


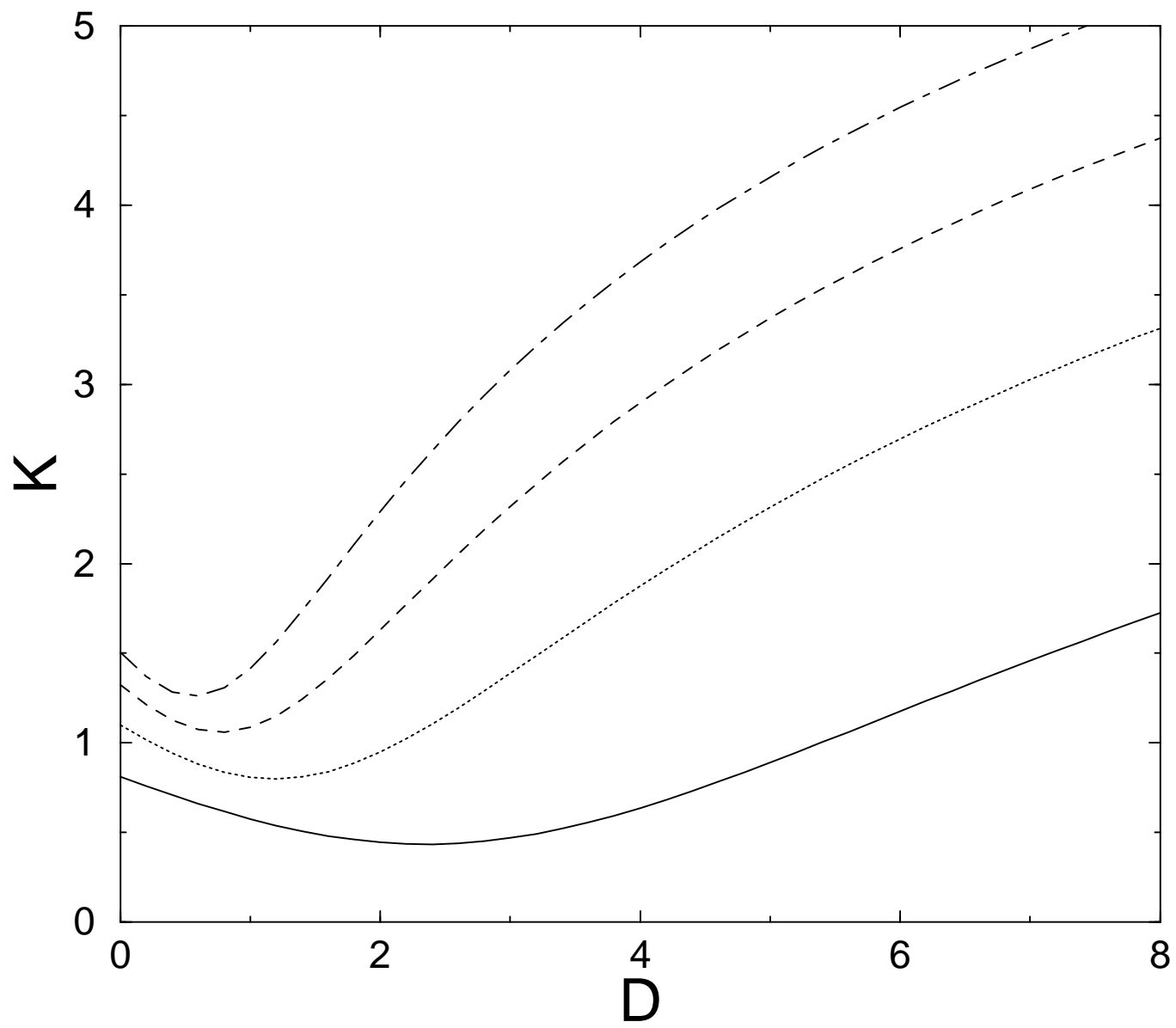


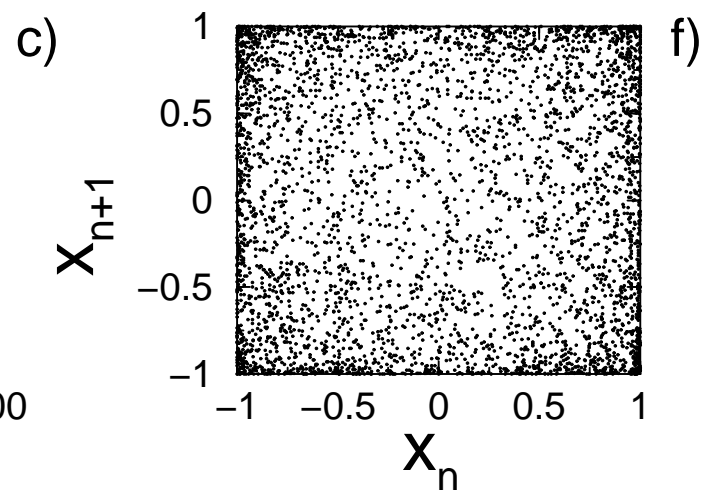
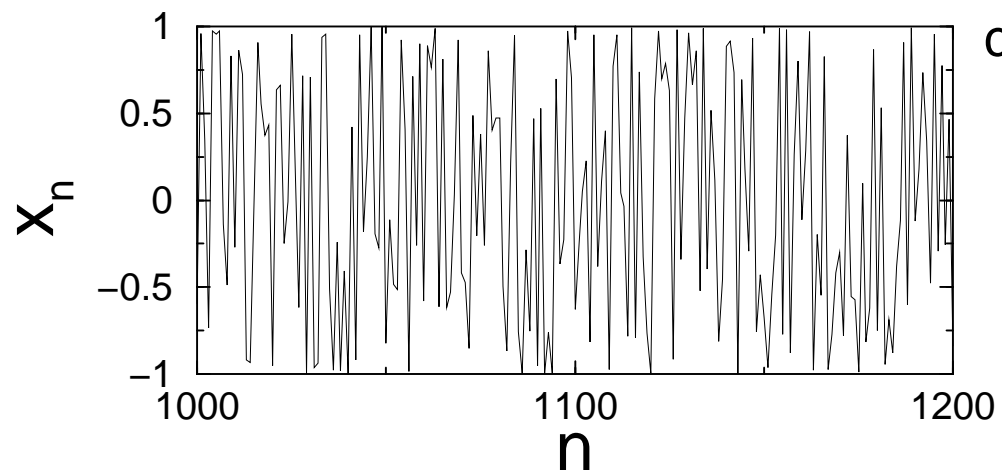
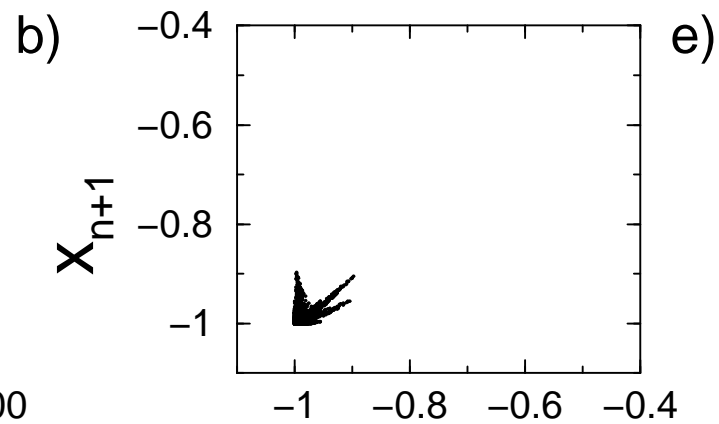
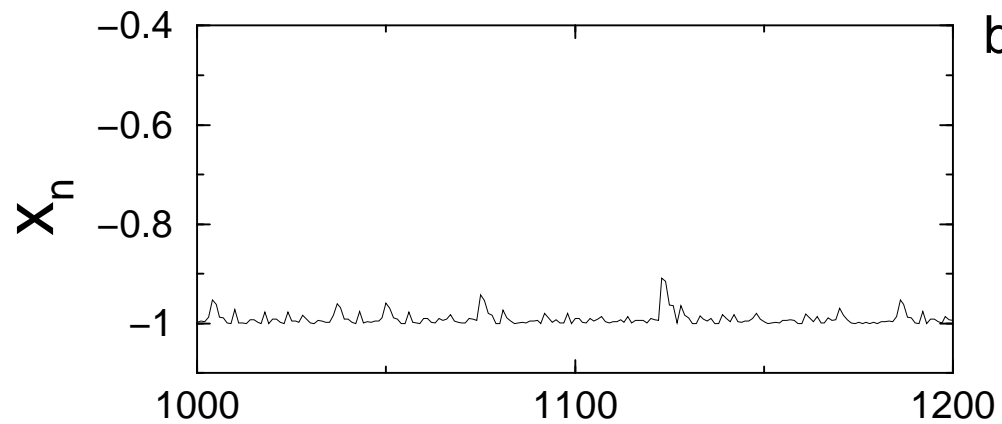
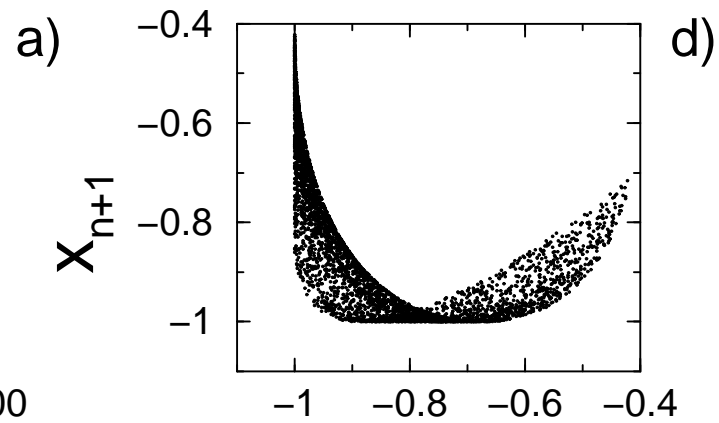
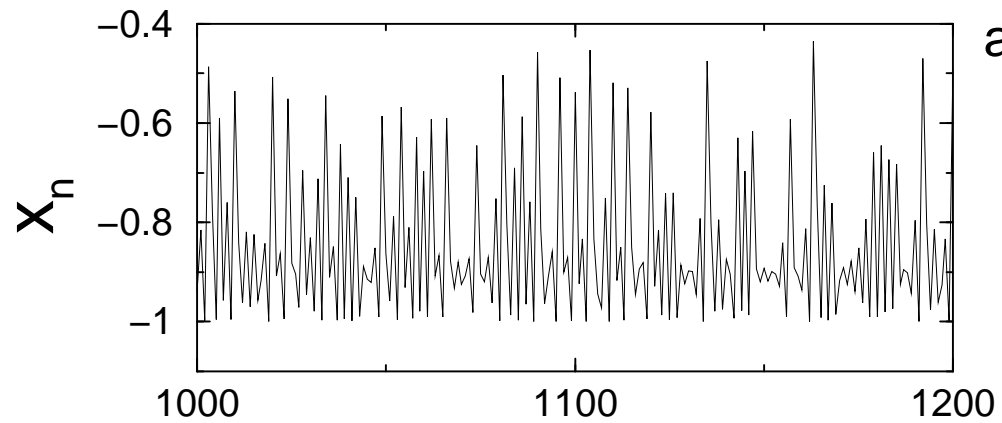


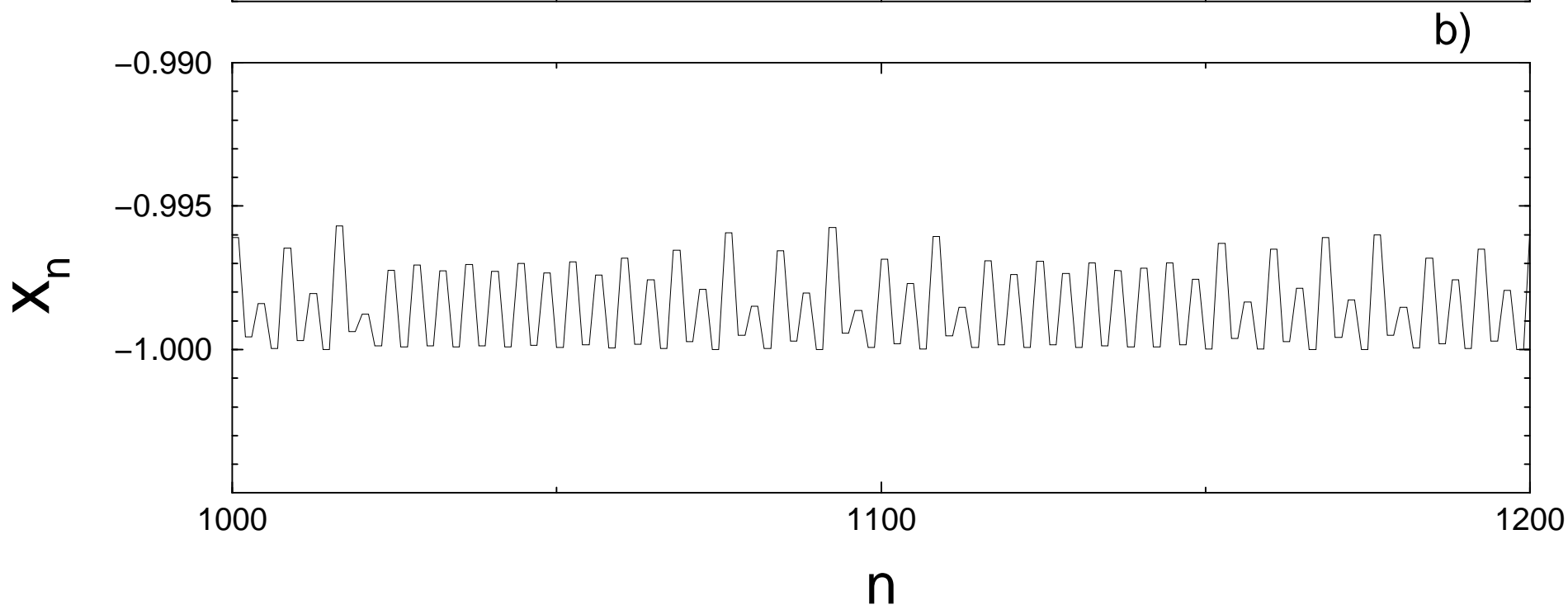
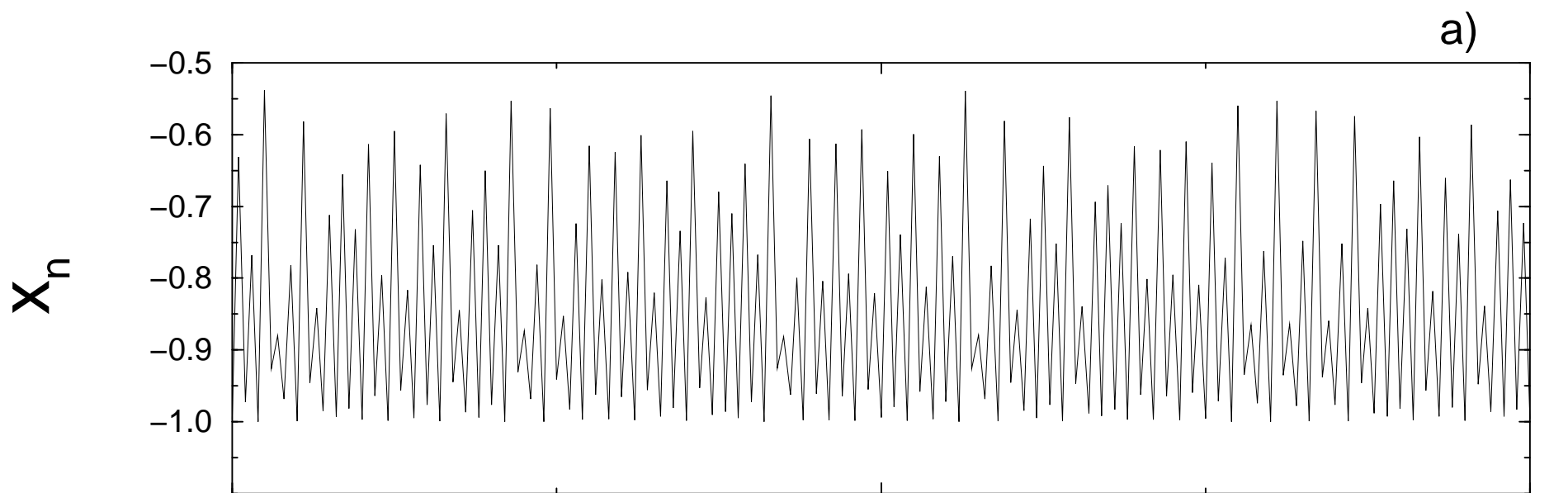


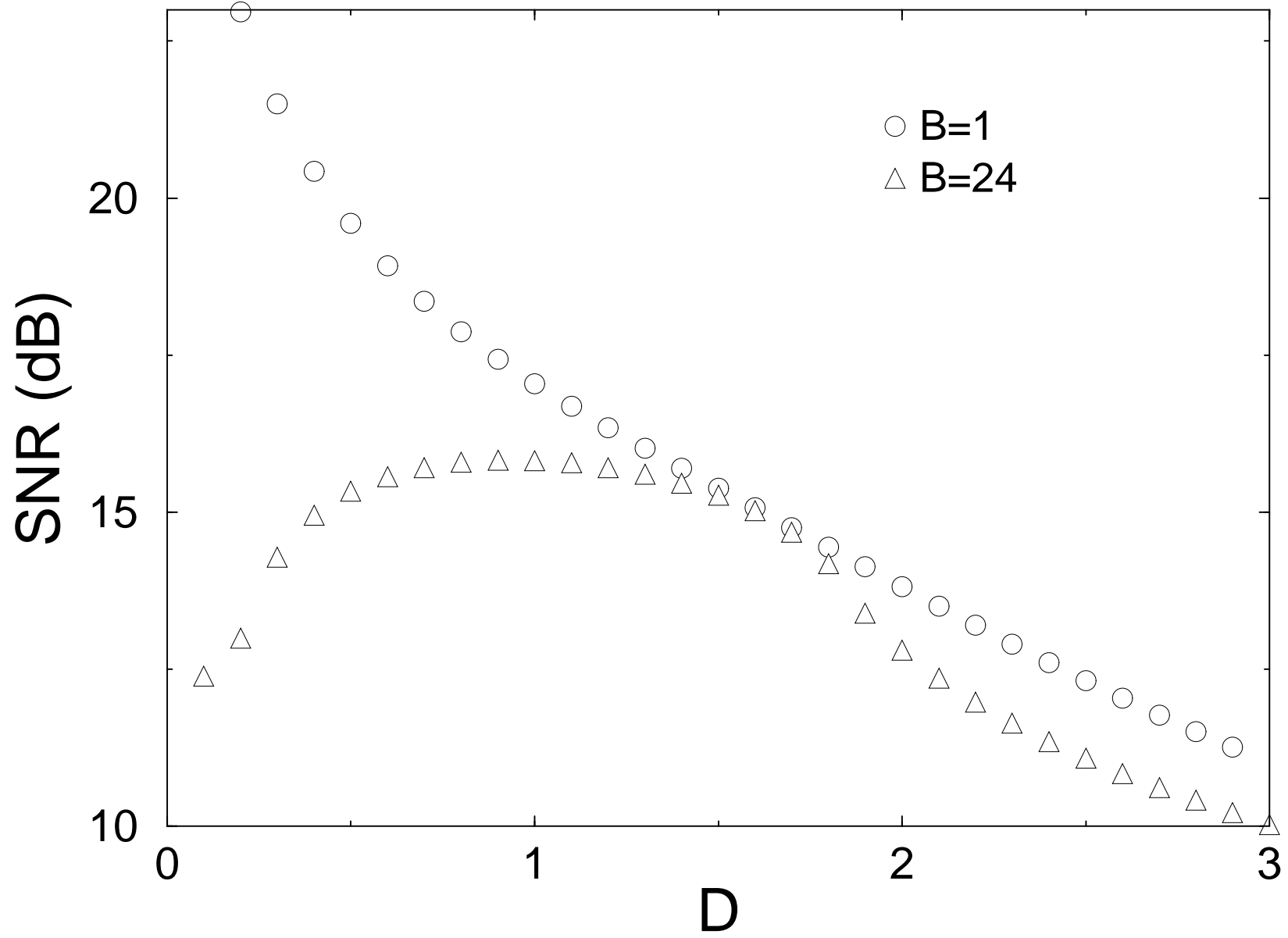


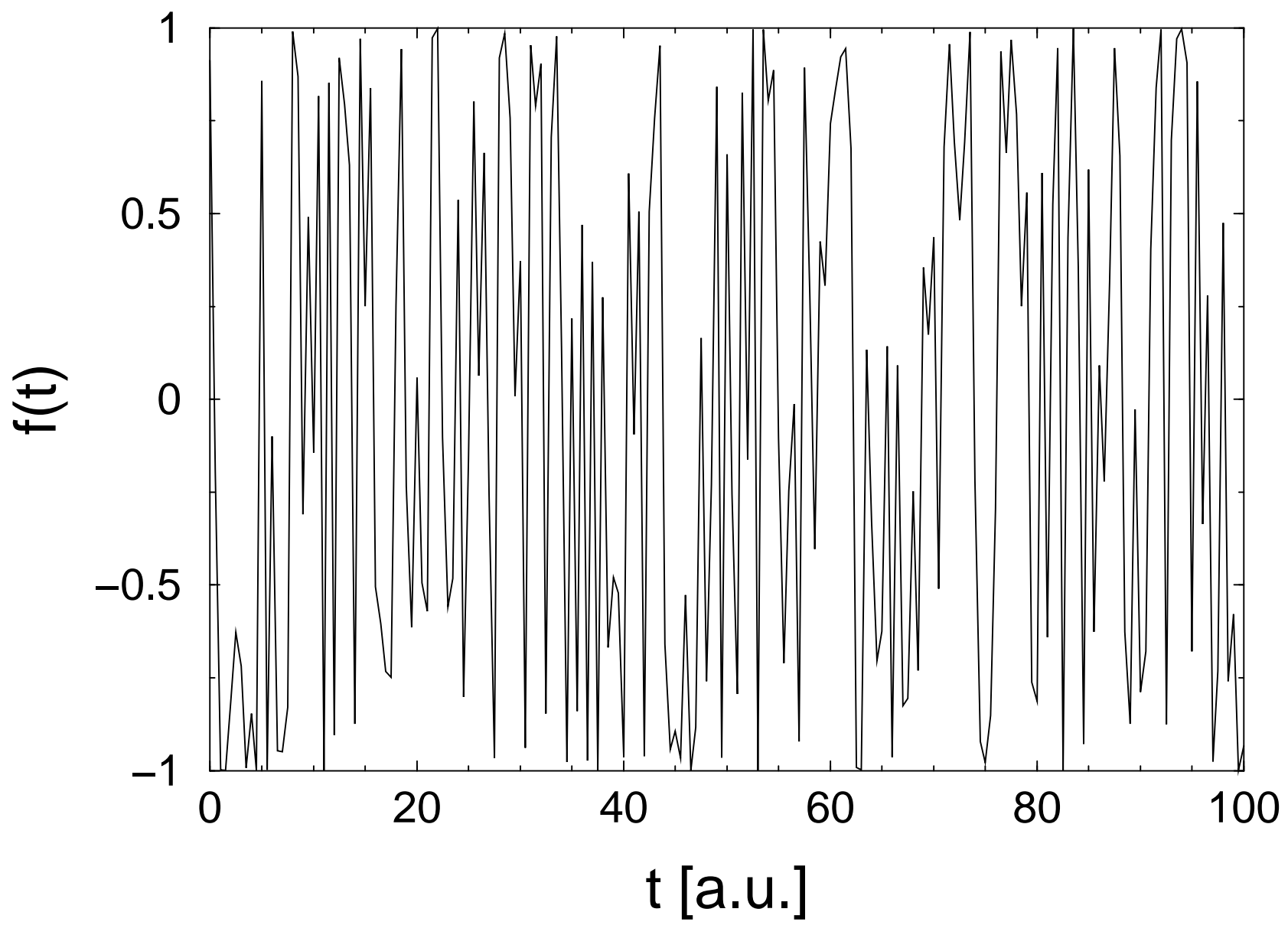


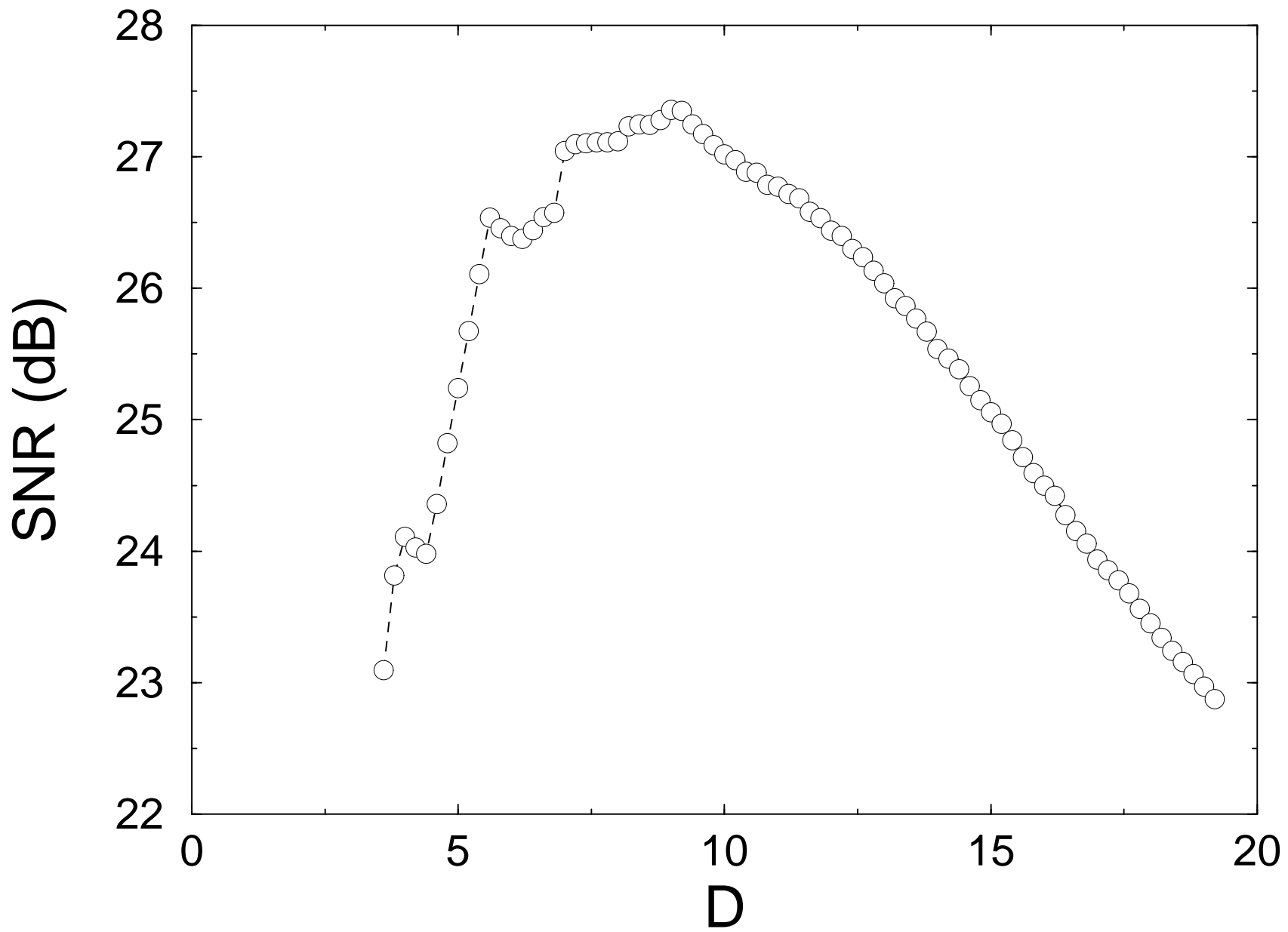


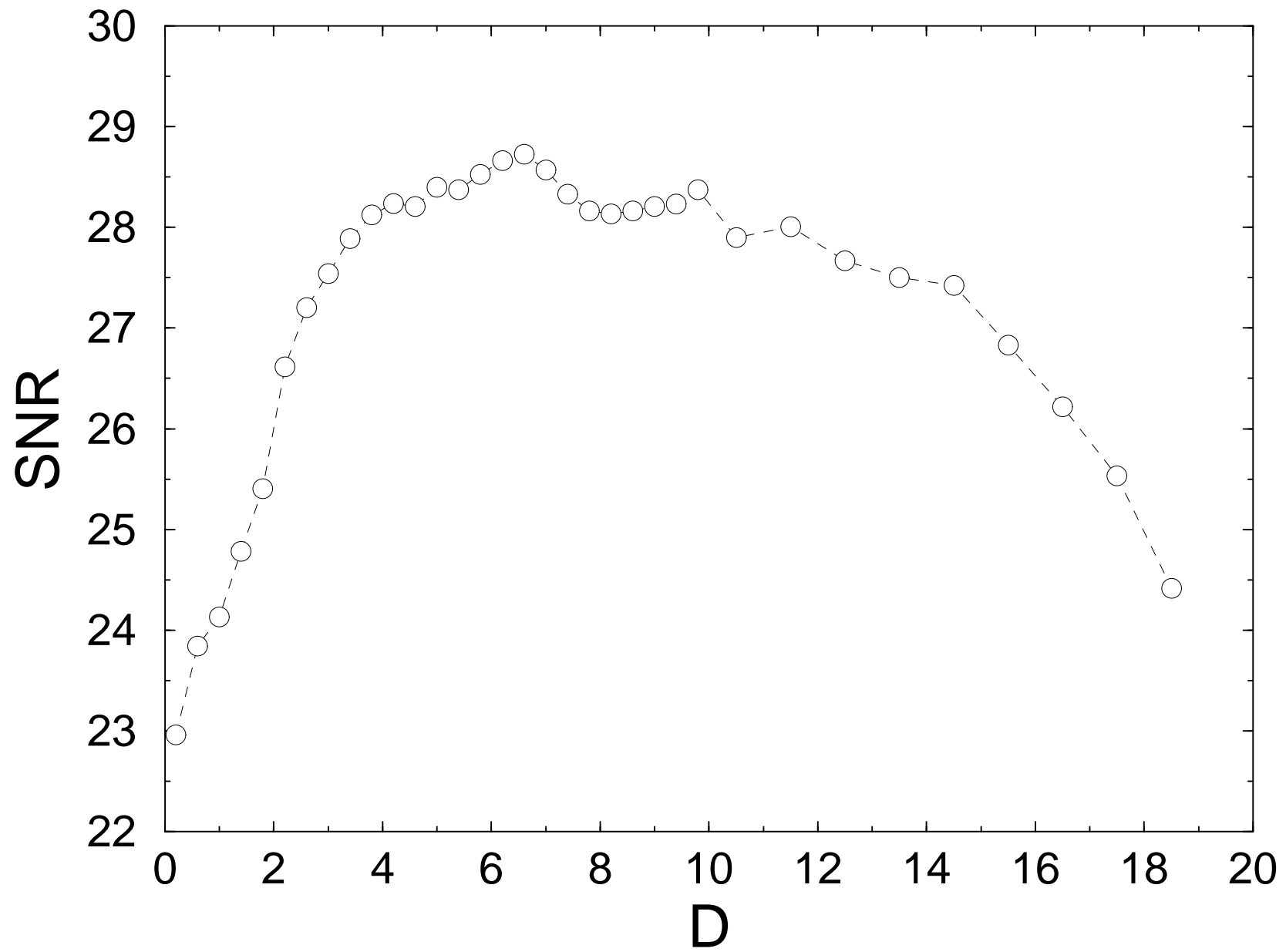


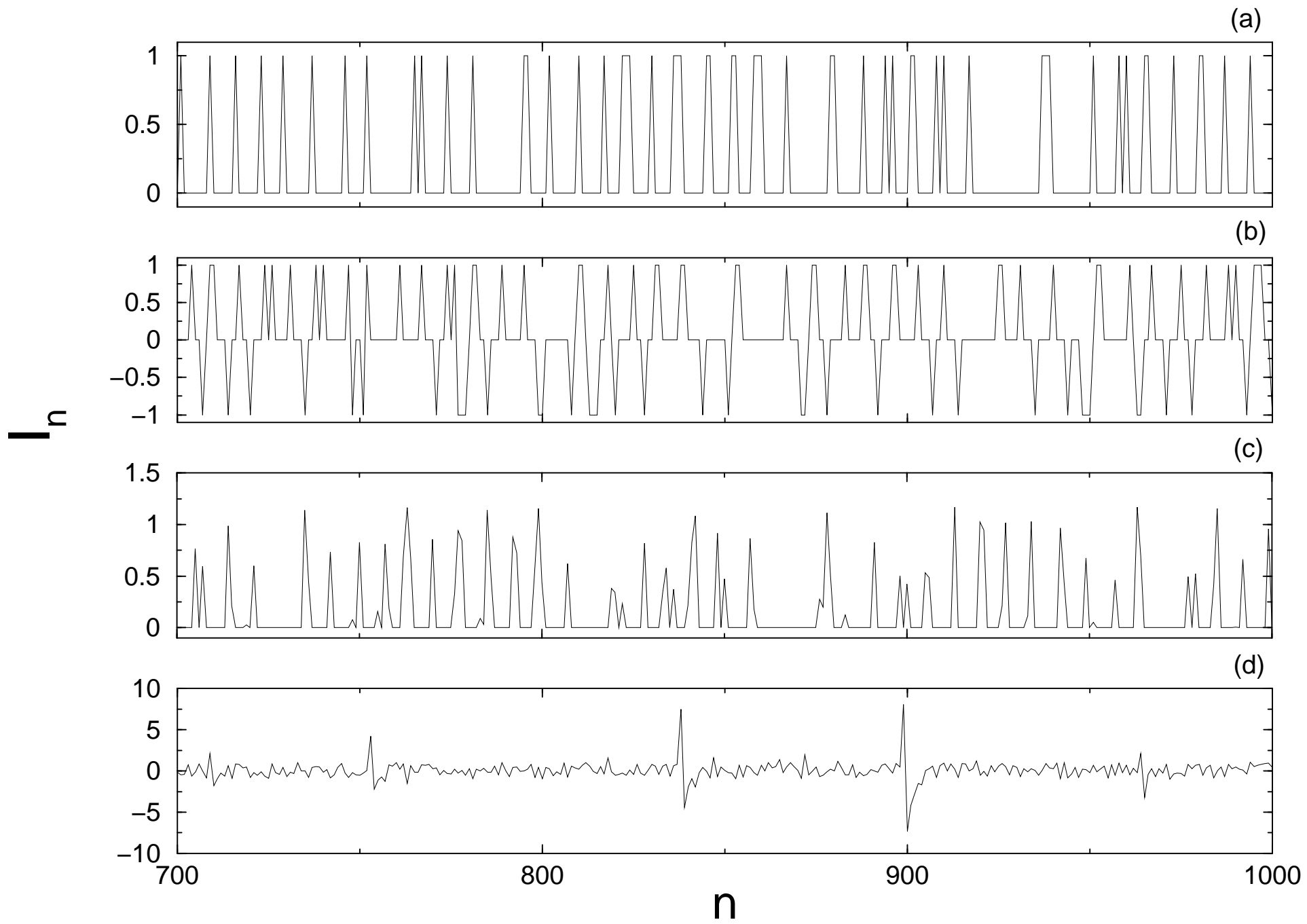


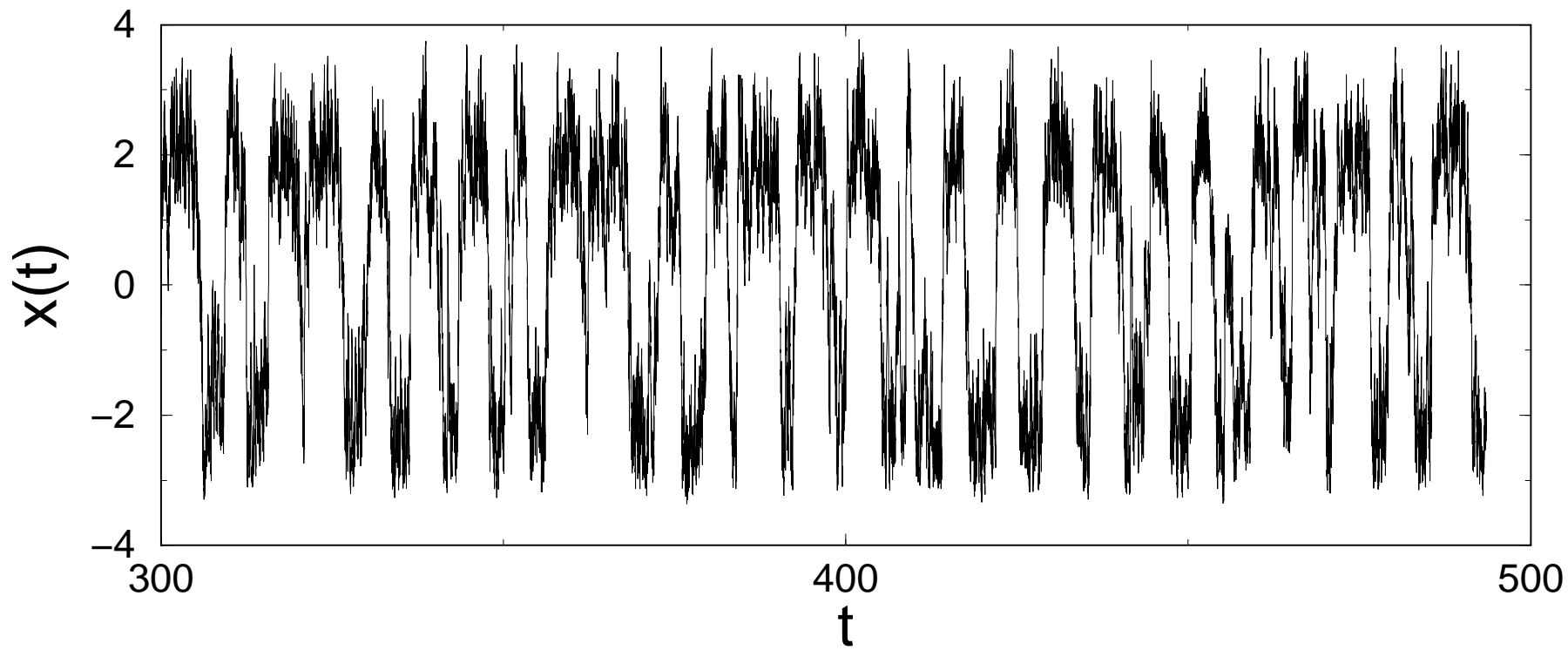




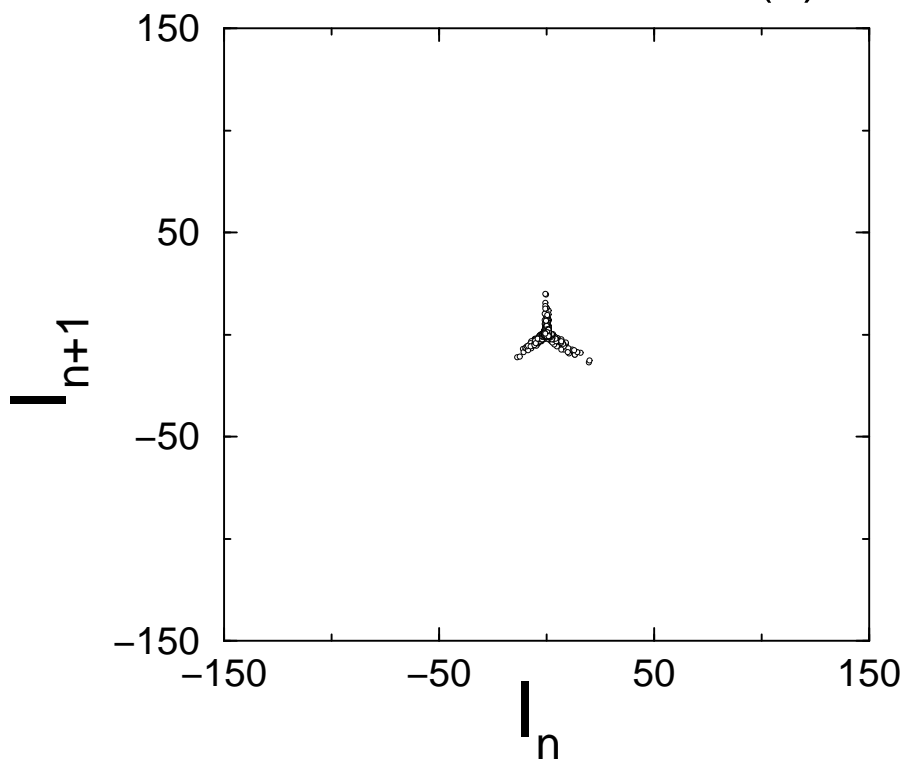




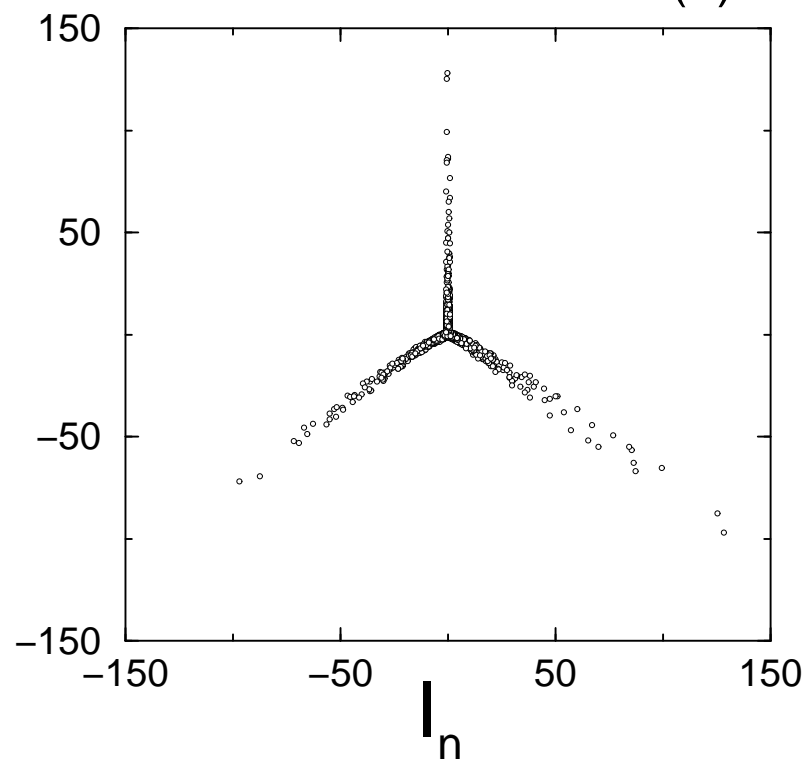




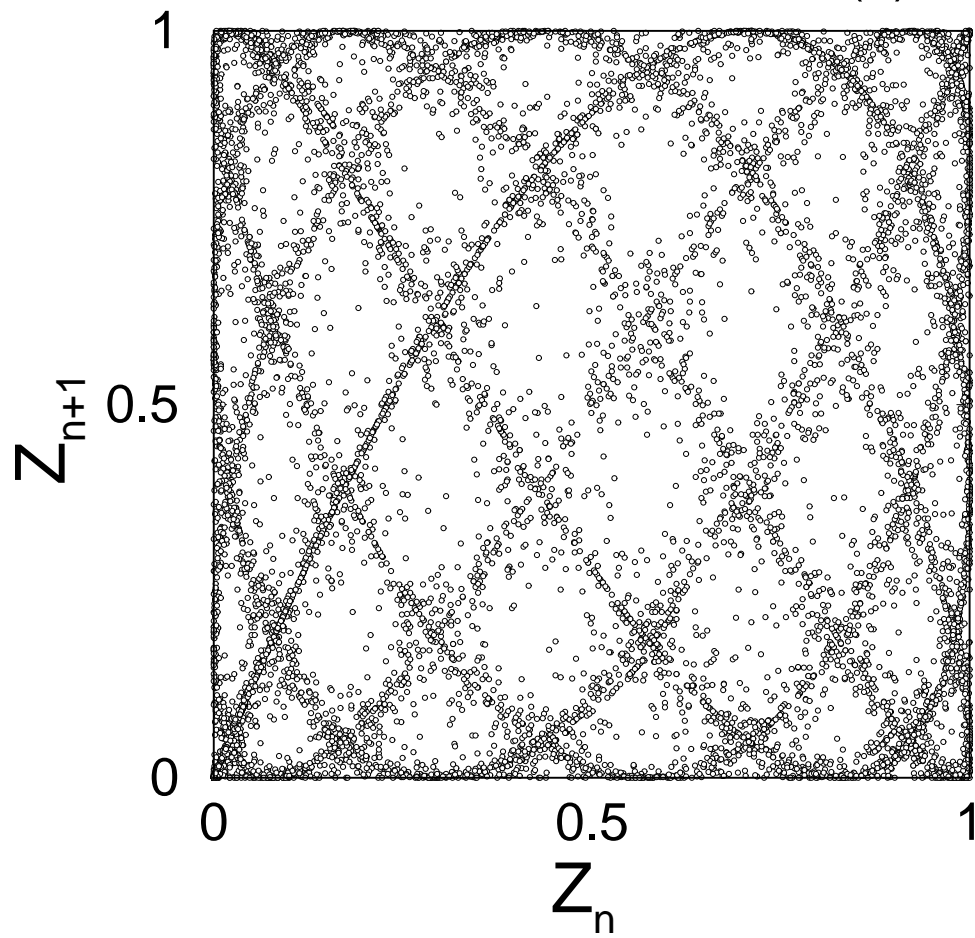
(a)



(b)



(a)



(b)

